

N71-25962
NASA CR-118643

TM-71-1011-4

**TECHNICAL
MEMORANDUM**

**AN ANALYTICAL MODEL OF ECLIPSING
BINARY STAR SYSTEMS**

**CASE FILE
COPY**

Bellcomm

BELLCOMM, INC.

955 L'ENFANT PLAZA NORTH, S.W., WASHINGTON, D.C. 20024

COVER SHEET FOR TECHNICAL MEMORANDUM

TITLE--An Analytical Model of Eclipsing
Binary Star Systems

TM-71-1011-4

FILING CASE NO(S)--105-9

DATE--April 16, 1971

AUTHOR(S)--D. B. Wood

FILING SUBJECT(S) Astronomy
(ASSIGNED BY AUTHOR(S))-- Eclipsing Stars

ABSTRACT

This report describes a new approach to the modeling of eclipsing binary star systems. Modern observational and analytical tools, including photomultiplier tubes, extremely stable voltage supplies and amplifiers, and digital computers, provide the possibility of obtaining and analyzing highly accurate light versus time curves of such eclipsing stars.

The analysis of eclipsing binary stars provides our primary source of knowledge about the physical properties of stars - mass, radius, luminosity, density and intensity gradients.

Currently, the main limitation on photometric accuracy is the variability of the properties of the earth's atmosphere. Telescopes located in space should be able to provide photometric accuracy which is limited only by the intrinsic capability of the photon detectors.

The current approach to analyzing eclipsing binary light curves is with a model developed more than half a century ago. Modern observations are approaching an accuracy greater than that of this model, and space-based observations will far exceed the precision of this technique.

The model described in this report takes advantage of a digital computer and thus allows a reduction in the number of simplifying assumptions. The validity of this model is tested through analysis of numerical integration errors, comparison with the spherical model, parametric studies, and application to observational data. It is concluded that the model is a valid representation of eclipsing systems, and that it is a useful tool for the analysis of such systems.

BA-145A (8-68)

DISTRIBUTION

COMPLETE MEMORANDUM TO

CORRESPONDENCE FILES:

OFFICIAL FILE COPY

plus one white copy for each
additional case referenced

TECHNICAL LIBRARY (4)

NASA Headquarters

- W. O. Armstrong/MTX
- P. E. Culbertson/MT
- C. J. Donlan/MH
- E. W. Hall/MTG
- H. Hall/MT-2
- T. A. Keegan/MA-2
- A. S. Lyman/MR
- G. K. Oertel/SG
- W. Quintrell/DHC-4
- N. G. Roman/SG
- J. W. Wild/MTE

GSFC

- K. L. Hallam/613
- S. Sobieski/613
- W. L. Stroud/110
- A. B. Underhill/613

MSC

- K. Henize/CB
- Y. Kondo/TG4
- T. L. Page/TG4

University of Florida

- J. E. Merrill
- F. B. Wood

University of South Florida

- E. J. Devinney
- R. E. Wilson

COVER SHEET ONLY TO

- J. P. Downs
- R. L. Wagner

COMPLETE MEMORANDUM TO

University of Georgia

- E. G. Reuning

Dominion Astrophysical Observatory

- G. Hill

University of Wisconsin

- J. E. Forbes

University of California, Berkeley

- H. S. Spinrad

University of Pennsylvania

- R. H. Koch

U.S. Naval Observatory
Flagstaff Station

- R. L. Walker, Jr.

University of California at
Los Angeles

- M. Plavec

BELLCOMM. INC.

Subject: An Analytical Model of
Eclipsing Binary Star
Systems - Case 105-9

Author: D. B. Wood

DISTRIBUTION LIST (cont'd)

Bellcomm, Inc.

A. P. Boysen, Jr.
A. C. Buffalano
D. R. Hagner
N. W. Hinners
D. P. Ling
H. S. London
J. Z. Menard
G. T. Orrok
J. W. Timko
M. P. Wilson

All Members, Dept. 1011, 1013, 2015
Department 1014 Supervision
Department 1015 Supervision
Center 201 Supervision
Department 1024 File

SUBJECT: An Analytical Model of Eclipsing
Binary Star Systems - Case 105-9

DATE: April 16, 1971

FROM: D. B. Wood

TM-71-1011-4

TECHNICAL MEMORANDUM

I. INTRODUCTION

Knowledge about the physical properties of stars is crucial to understanding their energy generation, radiative processes, and evolutionary cycle. Such quantities as mass, radius, surface temperature, luminosity, density gradient, variation in intensity across the surface, etc. are known in detail for only one star - our sun. The main source of information for other stars comes from the study of various classes of double stars - two stars in orbital motion about their common center of gravity.

- Visual double stars are widely enough separated so that their orbital motion, projected on the "plane of the sky", may be followed. Separations vary from several seconds of arc down to the resolution limit set by the telescope and the Earth's atmosphere. Periods vary from about five years up to thousands of years. If the distance to the double star system can be determined, then the masses and intrinsic luminosities (absolute magnitudes) can be determined.

- Spectroscopic binary stars are double stars which have a large enough orbital velocity component in the line of sight to produce a measurable change in the Doppler shift of lines in the spectrum. Orbital velocities vary from nearly 500 km/sec down to the limits of measurements, a few km/sec. Periods range from a few hours to more than a decade. A few spectroscopic binary stars are visual double stars, but the vast majority are unresolvable. If the two stars are quite comparable in brightness, then each star can be detected by the periodic doubling of the spectral lines, as one star approaches us and the other recedes. In most cases, however, only one of the two stars is visible spectroscopically and one sees its absorption lines periodically shifting redward and blueward. Not much information is available from these single-line (one spectrum) binaries, but the masses of double-line (two spectrum) binaries can be determined if the inclination of the plane of the orbit can be determined. The inclination (angle between the orbital plane and the plane of the sky) can be found if the spectroscopic binary is also a visual double star or an eclipsing binary star.

Eclipsing binary stars are spectroscopic binary stars which have orbital plane oriented in such a way (inclination near 90°) that they nearly include the earth. Hence the observed luminosity of the unresolved stars is periodically reduced as the stars alternately eclipse each other. The study of the light curves (intensity vs time) of eclipsing binaries gives us our greatest knowledge about the physical properties of stars. Figure 1 shows a typical light curve. The ordinate of a light curve may be expressed in actual time units or, equivalently, in orbital longitude (0° to 360°) or phase (0 to 1). We can determine the relative radii of the two stars (in terms of their separation), their physical distortion (which is related to density distribution), their limb darkening (decrease of intensity from the center to the limb), their relative brightness, and such interactive phenomena as reflection (the heating of one star by the other). If the star system is a double-line, spectroscopic, eclipsing binary, the radii can be expressed in absolute units and the masses determined.

The experimental precision of these light curves depends on instrument sensitivity and on night to night reproducibility. The introduction of photomultiplier tubes and stable electronic has improved precision until it is now limited by the variability of the atmosphere. Space-based telescopes such as those planned for the shuttle and space station program will provide a major advance in data gathering, eliminating atmospheric limits associated with Earth-based telescopes. This report describes a method of analyzing light curves with great precision.

II. BACKGROUND

The traditional approach to the solution for the physical parameters of eclipsing binary stars has been based on the mathematical simplicity of the "spherical model", in which the stars are assumed to be perfect spheres. H. N. Russell⁽¹⁷⁾ developed this elegant approach to what would have otherwise been an intractable problem. Many methods of application of this model have been developed; the most notable being that of Russell and Merrill⁽¹⁹⁾ and that of Kopal⁽⁸⁾. The Kopal method is an iterative procedure and lends itself well to computer application (e.g., Jurkevich⁽⁷⁾, Huffer and Collins⁽⁶⁾). These⁽¹⁶⁾ methods require either extensive tables, as generated by Merrill⁽¹⁶⁾ and Tsesevich^(21,22), or special functions generated by the computer during solution (Jurkevich⁽⁷⁾ and Linnell⁽¹⁰⁾). In all cases, however, the use of the computer has still been tied to the spherical model.

A more powerful application of the computer would be to discard the spherical model and the dubious procedure of rectification* by taking into account in a more exact manner the complexities of binary stars. The usual perturbations of the spherical model can be represented by straight-forward physical models. Thus it is now reasonable to build, in a computer, a detailed model of an eclipsing binary system and study with great accuracy the effects of non-sphericity, gravity brightening, reflection, limb darkening, and orbital eccentricity. Recently, this straight-forward approach has been investigated in various aspects (Lucy⁽¹⁴⁾, Hill and Hutchings⁽⁵⁾, Cochran⁽³⁾).

The procedure discussed herein was first described conceptually at the Berkeley meeting of the IAU⁽²⁴⁾. However, the approach proved too ambitious for computers of that era.

III. THE MODEL

This model of eclipsing binary systems takes into account the best understood geometric and photometric distortions, including limb darkening, gravity brightening, and reflection. Other important perturbations, such as gas-streaming, are much more complex in nature and are not considered at this time.

The photospheric surface of each star is assumed to be representable by a tri-axial ellipsoid, with the major axes pointing toward each other at periastron. The orbit may be eccentric, and the stars rotate in their orbital plane with a period equal to the orbital period. It is presumed that tidal forces between two close stars will have forced the period synchronism and the coplanar rotation. The model is described by the following parameters:

Orbital Parameters

Period of revolution	P
Time of conjunction	T_c
Semi-major axis of orbit	R_o

*An important aspect of the spherical model is the reduction of distorted stars to spheres by "rectification". The out-of-eclipse light variation is analyzed for its Fourier harmonics, and the entire light curve is rectified by the addition of and division by appropriate Fourier coefficients. Rectification also removes reflection effects.

Orbital eccentricity	e
Longitude of periastron	ω
Inclination	i

Geometric Parameters

Semi-axes of star "A"	a_A, b_A, c_A
Semi-axes of star "B"	a_B, b_B, c_B

Photometric Parameters

Surface intensity (defined below)	\bar{I}_A, \bar{I}_B
Limb darkening coefficient	u_A, u_B
Gravity brightening coefficient	v_A, v_B
Reflection coefficient (albedo)	w_A, w_B

A. Orbital Parameters

The orbital parameters are defined in the usual sense for binary star orbits (see Figure 2). In order to avoid the ambiguity in ω as e approaches zero, e and ω are always used in the combinations $e \sin \omega$ and $e \cos \omega$.

B. Geometric Parameters

Chandrasekhar⁽¹⁾ showed that, to third order in v^* , a tidally distorted rotating polytrope could be approximated by a tri-axial ellipsoid. For very close stars ($v \approx 1/2$), ignoring higher terms in v produces deviation from theory in the semi-major axis of about 6% for stars of equal mass.

It is important to note three important considerations which relate to the use of a tri-axial ellipsoid in this model. First, there is no relationship between the use of an ellipsoid in this context and the use of the "ellipsoidal model" in rectification. In the latter case the isophotes are concentric, similar ellipses, which is far from the real situation (see Figure 3). Second, there is no a priori reason to assume that

$$*v = \frac{\text{radius of unperturbed star}}{\text{separation of centers}}$$

the photospheres of distorted, turbulent stars are any better represented by another form, such as the often-cited Roche model. Other, complex, configurations are discussed in the work of Kopal⁽⁹⁾, Lucy⁽¹³⁾, and Martin⁽¹⁵⁾, which suggests there is a variety of proposed star shapes to choose from. Third, given this variety of shapes, the ellipsoid is very attractive from a computational point of view. The fact that an ellipsoid projects on the plane of the sky as an ellipse is particularly useful in performing accurate eclipse integrations.

The two stars are not identified in the usual way as "larger" and "smaller", but rather as star "A" and star "B". Star A is eclipsed at the deeper eclipse and is considered to be the central star about which B revolves.

It is convenient to replace the six geometric parameters (the star axes) with six dimensionless parameters.

$$a, k, \epsilon_A, \epsilon_B, \zeta_A, \zeta_B,$$

which are related to the actual axes by the following:

$$\begin{aligned} a_A &= aR_0 \\ a_B &= kaR_0 \\ b_A &= \epsilon_A aR_0 \\ b_B &= \epsilon_B kaR_0 \\ c_A &= (1 + \zeta_A) \epsilon_A^2 aR_0 \\ c_B &= (1 + \zeta_B) \epsilon_B^2 kaR_0 \end{aligned} \tag{1}$$

The ϵ are the ellipticities in the a-b (orbital) plane and the ζ measure how much the ellipticity in the b-c plane differs from that. The parameter k is defined in a slightly different manner than it is for the spherical model. By defining k as the ratio of the semi-major axis of star B to that of star A, k can be greater than unity if star B is the larger. Hence primary eclipse is an occultation if $k > 1$ and a transit if $k < 1$. The semi-major axis of the orbit, R_0 , is used as the unit of length, so that "a" represents the semi-major axis of star A in dimensionless units.

From the work of Chandrasekhar⁽¹⁾ we could express the six axes of the stars as functions of a , k , the mass ratio, and the polytropic indices. For generality, however, in this model the additional degrees of freedom provided by separate ϵ_A , ϵ_B , ζ_A , and ζ_B are retained in lieu of the mass ratio. The star shapes are described in greater detail in Appendix A.

C. Photometric Parameters

Limb darkening is expressed here by the usual linear law

$$I = I_0(1 - u + u \cos \gamma) \quad (2)$$

where γ is the foreshortening angle and u is the limb darkening coefficient. I_0 is the intensity of the "sub-earth" point, where the line of sight from the observer is normal to the stellar surface and $\gamma = 0$. For a distorted star, this point is generally not at the center of the apparent disk. Isophotes, contours of constant γ , are not similar ellipses for an ellipsoidal star, as was shown in Figure 3.

The relative surface intensities of the two stars cannot be uniquely defined in the same way as is possible for spherical stars, since the apparent brightness is constantly changing with orbital phase. Thus the intensity ratio, j , is defined at time $= T_Q = T_C + P/4$ as

$$j = \bar{I}_B / \bar{I}_A \quad (3)$$

where \bar{I} is the value of I_0 at quadrature.*

The gravity brightening coefficient, v , is defined to be like limb darkening, so that

$$I_0 = \bar{I}(1 - v + v \frac{r}{r}) \quad (4)$$

*For circular orbits T_Q is time of quadrature. Although this is not generally true for eccentric orbits, the term "quadrature" will be used to describe $T_C + P/4$.

where r is the local radius and \bar{r} is radius to the sub-earth point at quadrature, where \bar{I} is defined. The derivation of Equation (4) is outlined in Appendix B. The parameter v is the negative of b as defined by Kopal⁽⁸⁾. If local flux varies directly as local gravity⁽²⁷⁾, then v is approximately -4. If flux is less sensitive to local gravity, as suggested by Lucy⁽¹²⁾, then v may be more like -1.5.

Two stars very close together will heat each other so that the intrinsic radiation, I_o , is in effect augmented by radiation which is "reflected". In the present model, reflection effect is included as an albedo parameter, w , so that the total reflected light is just w times the integrated incident light. In any restricted spectral region, w may be more or less than unity, since reflection will generally involve a redistribution of spectral energy. Earlier treatments of reflection have contained many simplifying assumptions due to the complex geometry which was used, especially in the penumbral regions where the source star is partially below the local horizon (e.g., Russell⁽¹⁸⁾ and Kopal⁽⁸⁾). The geometric complexities are quickly removed, however, by a simple vector treatment of the problem (Chen and Rhein⁽²⁾ and Wood⁽²⁵⁾).

At the present, a more accurate astrophysical treatment of reflection, such as that used by Hill and Hutchings⁽⁵⁾, is not considered to be useful. The computation of reflection has such a major impact on the running time of any computer program which calculates light curves, that low-accuracy integration schemes must be used. The trade-off is generally between accurate integration of a simple reflection model or poor integration of a sophisticated reflection model. In truth, neither model may represent the true effect in a turbulent atmosphere.

The photometric parameters are described in more detail in Appendix B.

D. System Luminosity

The total observed luminosity of a star is thus given by an integral over the apparent disk:

$$L = \iint (I_o + I^*) (1 - u + u \cos \gamma) dA , \quad (5)$$

where I_0 is the normal emergent intensity given by Equation (4) and I^* is the normal component of the reflected intensity, given by

$$I^* = wL^*/2\pi(1 - u/2). \quad (6)$$

L^* is the incident flux from the other star, found from an Equation like (5), but which takes into account the unique geometry (see Appendix B). The total system luminosity at any time t is

$$L_{TOT}(t) = L_A(t) + L_B(t) - L_E(t) \quad (7)$$

where the light lost in eclipse, L_E , is found from Equation (5), integrated over the overlapping area. The system luminosity is normalized at quadrature; $L_{TOT}(T_Q) = L_A(T_Q) + L_B(T_Q) = 1$. Because of this normalization, both surface intensities, \bar{I}_A and \bar{I}_B , are determined by j (Equation (3)).

IV. VERIFICATION OF THE MODEL

It is impossible to prove the "accuracy" of the model, but its validity can be checked in a variety of ways, including application to real eclipsing systems.

A. Accuracy of Numerical Integration

Numerical integrations are performed using the Gauss quadrature method. Table 1 shows the accuracy of the integration compared to the exact integration for a spherical star*. Numerically, the same accuracy should prevail for distorted stars, however precise analytic analysis is not possible in general. For an undarkened ellipse, the intensity is just πab , and the accuracy of numerical integration agrees with that above. In the general case, we can express the error (in magnitudes) of the coarser integrations compared with the 16×16 integration. In Table I we have shown the mean systematic error (with respect to 16×16 integration) and the root mean square scatter about this mean. Since 10-point integration provides adequate accuracy for any graphical presentation, all results discussed in this paper will be based on that integrational accuracy.

*For a spherical star of radius r and no reflection, Equation (5) is exactly integrable to $L = I_0 \pi r^2 (1 - u/3)$.

B. Comparison with the Spherical Model

Using the alpha-function tables of Merrill⁽¹⁶⁾ primary and secondary eclipses were generated for a pair of limb-darkened spherical stars. The comparison with this model is shown in Table 2, where we see the largest deviation is about .0003.

It is possible to use this model to generate alpha-functions, using the relationships (in Merrill's notation)

$$\alpha^{\text{oc}}(x, k, p) = \frac{1 - 1^{\text{oc}}}{L_s} \quad (8)$$

$$\alpha^{\text{tr}}(x, k, p) = \frac{1 - 1^{\text{tr}}}{L_g \tau(u, k)} .$$

For primary eclipse as a transit, in the present notation Equations (8) become

$$\alpha^{\text{oc}}(u, k, p) = \frac{1 - L''}{L_B} \quad (9)$$

$$\alpha^{\text{tr}}(u, k, p) = \frac{1 - L'}{L_A \tau(u, k)} .$$

L' , the luminosity at time t in primary eclipse, and L'' , the luminosity at time $t + P/2$ in secondary eclipse are calculated from Equation (7). $\tau(u, k)$ is taken from Merrill's tables. Time t was chosen to provide even tabular values of p for comparison with tables. Spot checks of alpha functions generated in this manner with tabulations of Merrill⁽¹⁶⁾ and Linnell⁽¹¹⁾ for $u = .6$ show deviations of no more than $\pm .0002$. No better agreement can be expected with the integration accuracy used.

C. Parametric Studies

Examination of the effects of variation of isolated parameters can provide a great deal of insight into the operation of the model. Such investigations have proven invaluable in developing and "debugging" the computer program. A "standard" light curve (Figure 4) is adopted with the parameters listed in Table III, and we will examine the sensitivity to changes in a number of the orbital parameters.

Figure 5 shows the combined effects of ellipticity and gravity brightening. An increase in the gravity effect (a more negative v) looks very much like increased ellipticity. Because of this close coupling, it will probably be necessary to determine v from theory in most cases.

Figure 6 shows the effect of variation of the ratio of the radii through unity. The curve labeled 0.9 is a transit in primary eclipse, and the other curves are occultations. A change in k affects the depths of both eclipses and alters their widths.

Figure 7 shows the effect of reflection. The influence on the shoulder of primary eclipse is not perceptible on this scale, since the fainter star has a lesser influence on the brighter star. Curves are labeled by the value of $w/2\pi(1 - u/2)$. Thus 0.2 corresponds to an albedo of 0.88, and 0.4 to an albedo of 1.76. Figure 8 shows a detail of the shoulders of a much closer binary system. The unit albedo curve is about 0.03 magnitude brighter at phase .35 than at phase .15. Reflection effect introduces this distinctive asymmetry into the light curve.

Figure 9 shows the detail of the bottom of primary and secondary eclipse for a variety of limb darkening parameters. The depth of primary eclipse increases as the limb darkening of the secondary star is increased. The depth of secondary eclipse is likewise coupled to the limb darkening of the primary star. A novel feature is the shape of secondary eclipse (a transit) for zero limb darkening. For these ellipsoidal stars, the eclipsed area actually passes through a maximum about 0.01 in phase on each side of mid-eclipse.

Figure 10 shows the effect of variation of the radius of the primary star. Since the ratio of radii is fixed, the radius of the secondary star varies in the same sense. Eclipse depth is unchanged, but there is a strong effect on eclipse width. Notice that a 10% change in radius changes the steep portion of primary eclipse by more than 0.05 magnitude.

Figure 11 shows the effect of variation of the relative surface intensities. The brighter the secondary star, the more nearly equal are the eclipses. Notice also the effect upon reflection. For $j = .9$ the shoulder before primary eclipse is raised and that before secondary depressed.

Figure 12 shows the detail of the bottom of primary and secondary eclipse for small changes of inclination near 90° . As long as eclipse is total, its depth is unchanged. As long as limb darkening on the secondary star is not zero, the transit eclipses are changed in depth by a change in inclination.

D. Comparison with Observed Light Curves

The best test of the model is its ability to fit real, observed light curves. Here we show the results of trial-and-error fitting to observations of several eclipsing binaries.

1. VS Hydrae

The observations of VZ Hydrae were taken from Walker⁽²³⁾. His light curve is shown in Figure 1. There is no obvious interaction between the components, so the stars are taken to be spheres. Starting with Walker's elements, the parameters were adjusted to improve the fit in primary eclipse. The final fit to the V observations* is shown in Figure 13, and the elements listed in Table III. It is not surprising, but comforting to see that this model works for a real spherical system.

2. EG Cepheii

A more interesting test of the model is provided by application to this close system as observed by Cochran⁽⁴⁾. The V light curve shows no evidence of reflection effect. Figure 8 showed the effect of reflection for a system like EG Cep. The hotter star heats the facing side of the cooler star and this hot side comes increasingly more into view past phase .25, until it is eclipsed by the hotter star. Thus the system is appreciably brighter at phase .35 (and .65) than at phase .15 (and .85). This is not the case for EG Cep, so the V albedo is taken to be zero. Figure 14 shows the fit to the observations using this model and the parameters of Table III.

3. V1143 Cygni (HR 7484)

A good test of the ability of the model to handle eccentric orbits is provided by the system V1143 Cygni, as observed by Snowden and Koch⁽²⁰⁾. Their published elements were hardly changed to provide the fit shown in Figure 15. The values of $e \sin \omega$ and $e \cos \omega$ from Table III yield $e = .542$, and $\omega = 48.3^\circ$. Note that $k > 1$, so the comparable values normally published would be $a = .061$ and $k = .902$.

*"V" refers to a specific yellow filter passband in the standard (U,B,V) photometric system.

4. RU Ursa Minoris

Blue observations of RU Umi⁽²⁶⁾ were fit as shown in Figure 16 by the elements in Table III. This is a very close system which is very much like W Ursa Majoris systems. The normal spherical model is quite inadequate for handling such systems.

V. APPLICATION

At this point, we have established that the model reproduces the spherical model exactly for spherical stars, and that the model produces credible results for distorted systems. The model was based on a number of assumptions, such as synchronism of rotation and revolution. Using the existing model as a basic framework upon which to build, various effects not inherently part of the model can be investigated. In this manner, it may be possible to gain more insight into such effects as non-linear limb darkening, non-synchronism of rotation, atmospheric eclipses, reflection with the hot-spot not at the sub-stellar point, etc.

Another important application of the model will be in the actual solution of eclipsing systems. In this paper, real systems have been fit with a trial-and-error procedure. An algorithm which will allow automated solution in the computer is under development.

A. Atmospheric Eclipses

For a test of the effect of a "fuzzy" star edge, a star was given an absorbing atmosphere, specifiable by a scale height. Thus a light ray reaching the observer from the eclipsed star is attenuated:

$$J = J_0 e^{-\tau} \quad (10)$$

where J_0 is the emitted intensity and J is the received intensity. The optical depth is given by

$$\tau = \tau_0 e^{-r/h} \quad (11)$$

where τ_0 is the optical depth at the "surface", assumed to be $4/3$ for the limb. The apparent distance of the ray above the limb is given by r , and h is the scale height. For $h/a \lesssim .001$, the effect is hardly perceptible (for $k \gg .001$). Figure 17 shows the effect of this absorbing atmosphere for $h/a = .1$ and $h/a = .01$.

B. Phase of Reflection

The unequal heights of maxima observed in W Ursa Majoris systems are a particular problem to explain. Orbital eccentricity combined with reflection could produce unequal maxima. However, W UMa systems have nearly circular orbits, so such an effect would be very small. What these systems require to explain them is an effect that is different at each quadrature; the stars need to be hotter on one side than the other. A simple way to produce this effect in the model is to introduce a phase shift in the reflection effect. What would be the effect if Coriolis forces moved the "hot spot" away from the sub-stellar point? The asymmetry of this effect depends strongly on the relative intensities, j , and on the relative albedos, w_A and w_B . An example of the effect is shown in Figure 18 for reflection lead or lag of 10° and the elements indicated in Table III for "Phase Shift". The maxima differ in height by about 0.016 magnitude, and reverse roles dependent upon phase lead or lag. Normalization at phase .25 has forced all the effect into the maximum following secondary eclipse.

C. Skew Stars

The model assumes that the stars rotate in the orbital plane with the major axes aligned. Figure 19 shows the effect on the light if one star is inclined 5° to the orbital plane and has the major axis out of alignment by 5° . The rising and falling branches are made unsymmetric, but the heights of maxima are preserved.

VI. RELATION TO PHYSICAL PARAMETERS

The physical parameters which describe a star are its mass, radius, luminosity (energy output), temperature, density gradient, chemical composition, surface gravity, atmospheric turbulence, and others. These properties are determined through the combined results of spectroscopy and photometry. In particular, let us see how photometric determination of the light curve of an eclipsing binary can lead to the determination of the mass, radius, luminosity and temperature of two stars.

As described in the introduction, our best hold on these quantities is in the case of double-lined spectroscopic eclipsing binaries. Through radial velocity measurements (in km/sec) and application of Kepler's Law, we obtain $R_o \sin i$ in km and $(m_A + m_B) \sin^3 i$ in solar masses, where m_A and m_B are the masses of the two stars. Thus the combination of this information with the photometric solution gives us the stellar masses and axes in absolute terms. As is shown in Appendix A, the mass also is related to the stellar axes for close, interactive star systems.

The determination of luminosity and temperature is assisted by eclipsing binary solutions. The luminosity of a star is dependent upon its surface area and upon its temperature. If T_e is the effective temperature (i.e., the temperature of a black body energy curve which most nearly replicates the star's energy curve) then we can say

$$L \propto r^2 T_e^4 \quad (12)$$

The radius, r , is determined from the eclipsing binary solution. In the case of distorted stars, the calculation of surface area is more complex. The effective temperature is determined from spectrophotometry.

The following tabulation relates the model and physical parameters:

Model Parameters	Physical Parameters	Remark
$P, i, T_c,$ $e \sin \omega,$ $e \cos \omega, R_o$	$P, i, T_c,$ e, ω, R_o	Defines orbit shape and orientation in space. P, T_c, e, ω, R_o can be determined spectroscopically.
a, k, ϵ, ζ	a_1 ; unperturbed radius q ; mass ratio	Related through theoretical expressions [equation (A-2)].
j, u, v, w	T_e ; effective temperature P_e ; electron pressure P_g ; gas pressure κ_v ; absorption coefficient	Related through theoretical astrophysics: T_e, P_e, P_g and κ_v define a stellar atmosphere, and that atmosphere determines u, v, w and j .

VII. CONCLUSIONS

Conceptually, the model described herein is superior to the spherical model because it accounts in a more straight forward way for the "photometric perturbations" of the spherical model. In addition, the model has passed all parametric tests and has proven its ability to match observed light curves. We conclude that the model is a valid representation of eclipsing binary star systems, including very close systems.

Using this model as a tool, we can now attack the following problems:

- 1) Determine model parameters for observed systems, using an iterative least-squares technique.
- 2) Examine the effects of the model assumptions (e.g., coplanar rotation).
- 3) Examine the effects of other photometric disturbances, such as extended atmospheres and gas-streaming.
- 4) Examine the effect of more sophisticated reflection calculations.



D. B. Wood

1011-DBW-ulg

Attachments

Appendices A-C
References
Tables I-III
Figures 1-22

APPENDIX A

Ellipsoidal Star

1. Distorted Polytrope

A polytropic stellar model is one in which the radial density distribution is described by an exponent, n , called the polytropic index. Chandrasekhar⁽¹⁾ analyzed the distortions of such polytropes under the influence of rotation and tidal interaction. Let q be the mass ratio (perturbing star mass/perturbed star mass), a_0 be the radius of the polytropic sphere before distortion, and v be a_0 expressed in units of the star separation, R . Chandrasekhar showed that the deviations from the unperturbed sphere (radius a_0) could be expressed as

$$\left. \begin{aligned}
 \sigma_1 &= \frac{1}{6}(1 + 7q)\Delta_2 v^3 + q\Delta_3 v^4 + q\Delta_4 v^5 + \dots \\
 \sigma_2 &= \frac{1}{6}(1 + 7q)\Delta_2 v^3 - q\Delta_3 v^4 + q\Delta_4 v^5 + \dots \\
 \sigma_3 &= \frac{1}{6}(1 - 2q)\Delta_2 v^3 + \frac{3}{8}q\Delta_4 v^5 + \dots \\
 \sigma_4 &= -\frac{1}{3}(1 + \frac{5}{2}q)\Delta_2 v^3 + \frac{3}{8}q\Delta_4 v^5 + \dots
 \end{aligned} \right\} \quad (A-1)$$

where σ_1 is the extension in the equatorial plane toward the perturbing star, σ_2 is the diametrically opposite extension, σ_3 is the extension in the equatorial plane perpendicular to σ_1 and σ_2 , and σ_4 is the polar extension (contraction). The Δ_i are weak functions of the polytropic index, and are all near unity for the range of applicable indices ($3 \leq n \leq 5$). If terms in v^4 and higher are ignored, $\sigma_1 = \sigma_2$ and the star is a triaxial ellipsoid with axes given by

$$\left. \begin{aligned} a &= a_0 \left[1 + \frac{1}{6} (1 + 7q) \Delta_2 v^3 \right] \\ b &= a_0 \left[1 + \frac{1}{6} (1 - 2q) \Delta_2 v^3 \right] \\ c &= a_0 \left[1 - \frac{1}{3} \left(1 + \frac{5}{2} q \right) \Delta_2 v^3 \right] \end{aligned} \right\} \quad (A-2)$$

The error in the length of the semi-major axis in this ellipsoid approximation is approximately qv^4 . For extremely close stars ($v \approx .5$) the error is about 6% for unit mass ratio. Normally the value of v does not exceed .4, and the error for unit mass ratio would be less than 3%.

2. Coordinate Transformation

In a coordinate system with axes fixed in the star, the surface of the ellipsoidal star is given by

$$(x'/a)^2 + (y'/b)^2 + (z'/c)^2 = 1. \quad (A-3)$$

To determine the stellar eclipsed or uneclipsed intensity as seen by a distant observer, we are interested in the projection of this star on the "plane of the sky"; that is a plane tangent to the celestial sphere at the point where it is pierced by the observer's line of sight. If we define the $y-z$ plane as the plane of the sky, with the observer on the $-x$ axis, then the equation of the ellipsoid becomes

$$Ax^2 + By^2 + Cz^2 + 2Dxy + 2Eyz + 2Fxz = a^2 b^2 c^2 \quad (A-4)$$

where

$$\left. \begin{aligned} A &= b^2 c^2 \cos^2 \theta' \sin^2 i + a^2 c^2 \sin^2 \theta' \sin^2 i + a^2 b^2 \cos^2 i \\ B &= b^2 c^2 \sin^2 \theta' + a^2 c^2 \cos^2 \theta' \\ C &= b^2 c^2 \cos^2 \theta' \cos^2 i + a^2 c^2 \sin^2 \theta' \cos^2 i + a^2 b^2 \sin^2 i \\ D &= (b^2 c^2 - a^2 c^2) \sin \theta' \cos \theta' \sin i \\ E &= (b^2 c^2 - a^2 c^2) \sin \theta' \cos \theta' \cos i \\ F &= (b^2 c^2 \cos^2 \theta' + a^2 c^2 \sin^2 \theta' - a^2 b^2) \sin i \cos i \end{aligned} \right\} \quad (A-5)$$

θ' is the angle that the star has rotated from the line of sight (i.e., the angle between the projection of the $-x$ axis on the orbital ($x'-y'$) plane and the major ($+x'$) axis of the star); i is the orbital inclination.

The cosine of the angle between the line of sight and the normal to where it intersects the stellar surface (limb darkening angle) is given by

$$\cos \gamma = (Ax + Dy + Fz)/T \tag{A-6}$$

where

$$\begin{aligned} T = & [x^2(A^2 + D^2 + F^2) + y^2(B^2 + D^2 + E^2) + z^2(C^2 + E^2 + F^2) \\ & + 2xy(AD + BD + EF) + 2xz(AF + CF + DE) \\ & + 2yz(BE + CE + DF)]^{1/2} . \end{aligned} \tag{A-7}$$

To describe the star entirely in terms of plane-of-the-sky coordinates, equation (A-4) is solved for x :

$$x = -\frac{Dy + Fz}{A} + \frac{1}{A}[Ny^2 + Pz^2 + 2Ryz + S]^{1/2} \tag{A-8}$$

where

$$\left. \begin{aligned} N &= D^2 - AB \\ P &= F^2 - AC \\ R &= DF - AE \\ S &= Aa^2b^2c^2 . \end{aligned} \right\} \tag{A-9}$$

The outline of the "apparent" star (i.e., the projection of the star on the plane of the sky) is formed by setting $\cos \gamma = 0$ in Equation (A-6):

$$Ny^2 + Pz^2 + 2Ryz + S = 0 . \tag{A-10}$$

This is an ellipse with axes given by

$$a' = \left[\frac{2S}{-[(P - N)^2 + (2R)^2]^{1/2} - (P + N)} \right]^{1/2}$$

(A-11)

$$b' = \left[\frac{2S}{[(P - N)^2 + (2R)^2]^{1/2} - (P + N)} \right]^{1/2}$$

The integrations of Equation (5) are performed over this ellipse for calculation of total intensity. Integration of eclipsed intensity is over the area common to two intersecting ellipses.

APPENDIX B

Photometric Parameters

1. Limb Darkening

The linear limb darkening law (Equation (2)) is based on solution of the transfer equation for the case of radiative equilibrium in a stellar atmosphere which is, at least locally, plane parallel. It is normal to define the stellar surface at optical depth $2/3$ (i.e., where the attenuation of radiation is $e^{-2/3}$). In this case limb darkening is given by

$$I = I_0 (0.4 + 0.6 \cos \gamma) . \quad (B-1)$$

Equation (2) is a generalization of this solution which is linear, replacing the numerical coefficients with one general coefficient, u .

2. Gravity Brightening

The local effective temperature of a star is proportional to the local surface gravity:

$$T \propto g^\beta . \quad (B-2)$$

In 1924 von Zeipel⁽²⁷⁾ showed that the exponent was $1/4$. Recently Lucy⁽¹²⁾ calculated that when convection occurs in the outer layers of the star, β is more like 0.08.

We compare the local values of T and g to the mean values over the star, \bar{T} and \bar{g} :

$$\frac{T^{1/\beta} - \bar{T}^{1/\beta}}{\bar{T}^{1/\beta}} = \frac{g - \bar{g}}{\bar{g}} . \quad (B-3)$$

The flux of radiation from the star, at a particular wavelength, λ , is given by the Planck law:

$$J = 2hc^2 \lambda (e^{c_2/\lambda T} - 1)^{-1} \quad (B-4)$$

From the Planck law we can write an expression for J/\bar{J} , and perform a Taylor expansion for $T \sim \bar{T}$. In addition, equation (B-3) can be expanded for $T \sim \bar{T}$. If we eliminate the factor $(T - \bar{T})/\bar{T}$, which is common to these two series expansions, and ignore higher order terms, we get

$$J/\bar{J} \approx 1 + y \left(\frac{g - \bar{g}}{\bar{g}} \right) \quad (B-5)$$

where

$$y = \beta \frac{c_2}{\lambda \bar{T}} \frac{e^{c_2/\lambda \bar{T}}}{e^{c_2/\lambda \bar{T}} - 1} \quad (B-6)$$

From the work of Chandrasekhar⁽¹⁾ the surface gravity can be related to the radius:

$$\frac{g - \bar{g}}{\bar{g}} = \frac{r - \bar{r}}{\bar{r}} \left(\frac{\Delta_2 - 5}{\Delta_2} \right) \quad (B-7)$$

where Δ_2 is that defined in Appendix A. If we let

$$v = y \left(\frac{\Delta_2 - 5}{\Delta_2} \right) \quad (B-8)$$

then we have the gravity brightening law

$$J = \bar{J} \left(1 - v + v \frac{r}{\bar{r}} \right) \quad (B-9)$$

For convenience of the model, \bar{r} and \bar{J} are taken to be the values at the sub-earth point at quadrature. Notice that since $\Delta_2 \approx 1$, we can write

$$v \approx \frac{-4\beta a}{1 - e^{-a}} \quad (B-10)$$

where $a = c_2/\lambda T$. Thus v can be theoretically determined for any λ , given the effective temperature and the value of β .

3. Reflection Effect

The geometry of the reflection effect is shown in Figure 20. Consider the three unit vectors shown in the figure: \vec{v}_1 is the normal to area dA_1 on the reflecting star; \vec{v}_3 is the vector directed from dA_1 to area dA_2 on the source star; \vec{v}_2 is the normal to that area on the source star. For dA_2 to be visible from dA_1 (thus contributing to the reflection) the dot product $\vec{v}_1 \cdot \vec{v}_3$ must be positive and $\vec{v}_2 \cdot \vec{v}_3$ must be negative. The intensity received at dA_1 from dA_2 is found from considering the normal emergent intensity at dA_2 [Equation (4)], the limb darkening on the source star [Equation (2) with $\cos \gamma = |\vec{v}_2 \cdot \vec{v}_3|$], inverse square reduction of intensity at dA_1 , and the foreshortening angle for the incident flux (from $\vec{v}_1 \cdot \vec{v}_3$). The flux incident on dA_1 is thus given by

$$L^* = \iint I_{O2} [1 - u_2 + u_2 |\vec{v}_2 \cdot \vec{v}_3|] \frac{\vec{v}_1 \cdot \vec{v}_3}{d^2} dA_2 \quad (\text{B-11})$$

where d is the distance between dA_1 and dA_2 .

This energy is considered to be reflected isotropically over a hemisphere with an albedo w . The portion of this energy which is reflected normal to dA_1 is thus

$$I^* = w_1 L^* / 2\pi (1 - u_1/2) . \quad (\text{B-12})$$

The process is reciprocal, so star A illuminates star B and vice versa. Second order reflection is not included. That is, I_{O2} in Equation (B-11) is not augmented by light incident from star "1".

APPENDIX C

Orbital Mechanics

1. Basic Equations

The basic equations, which may be found in any celestial mechanics text, are given below. The mean anomaly is defined as

$$M = \frac{2\pi}{P} (t - T_0) \quad (C-1)$$

where T_0 is the time of periastron passage. The radius vector is defined as

$$R = R_0 (1 - e \cos E), \quad (C-2)$$

where $R_0 (\equiv 1)$ is the semi-major axis of the orbit and E is the eccentric anomaly, related to M by

$$E - e \sin E = M \quad (C-3)$$

The true anomaly is defined as (see Figure 21)

$$v = \frac{\pi}{2} - \omega + \theta \quad (C-4)$$

where θ , the orbital longitude, is measured from the line of sight ($\theta = 0$ at conjunction). The longitude of periastron, ω , is measured from the "entering" node, where the orbit crosses to the observer's side of the plane of the sky. The eccentric and true anomalies are related by

$$\left. \begin{aligned} \cos E &= \frac{\cos v + e}{1 + e \cos v} \\ \sin E &= \frac{\sqrt{1-e^2} \sin v}{1 + e \cos v} \end{aligned} \right\} \quad (C-5)$$

2. Derivation

• Time of Periastron

(C-4): At conjunction, $t = T_c$ and $\theta = 0$, so from Equation

$$v_c = \frac{\pi}{2} - \omega \quad (C-6)$$

so that equations (C-5) become

$$\left. \begin{aligned} \cos E_c &= \frac{\sin \omega + e}{1 + e \sin \omega} \\ \cos E_c &= \frac{\cos \omega \sqrt{1 - e^2}}{1 + e \sin \omega} \end{aligned} \right\} \quad (C-7)$$

Thus at conjunction Equation (C-3) becomes

$$\cos^{-1} \left\{ \frac{\sin \omega + e}{1 + e \sin \omega} \right\} - \frac{e \cos \omega}{1 + e \sin \omega} \sqrt{1 - e^2} = \frac{2\pi}{P} (T_c - T_o) \quad (C-8)$$

For the given $e \sin \omega$, $e \cos \omega$, T_c and P , Equation (C-8) is used to calculate T_o . The proper quadrant for the arccos is determined from the sign of

$$e \sin E = \frac{e \cos \omega \sqrt{1 - e^2}}{1 + e \sin \omega} \quad (C-9)$$

• Time Dependent Variables

Equation (C-3) is solved for E , using Equation (C-1) for a given t . The solution of (C-3), known as "Kepler's Equation", is iterated to convergence from

$$E_{i+1} = E_i + \frac{M - M_i}{1 - e \cos E_i} \quad (C-10)$$

which is conveniently written

$$\Delta E = \frac{e \sin E_i - E_i + M}{1 - e \cos E_i} \quad (C-11)$$

and convergence established when ΔE is sufficiently small.

The initial value of E is $E_0 = M_0 = M$ for small e .
If $e > .75$, $E_0 \approx (\pi+M)/2$.

Expansion of (C-4) in trigonometric functions yields

$$\left. \begin{aligned} e \sin \theta &= e \sin \omega \sin v - e \cos \omega \cos v \\ e \cos \theta &= e \sin \omega \cos v + e \cos \omega \sin v \end{aligned} \right\} \quad (C-12)$$

where $\sin v$ and $\cos v$ are found by inversion of Equations (C-5):

$$\left. \begin{aligned} \sin v &= \frac{\sqrt{1-e^2} \sin E}{1-e \cos E} \\ \cos v &= \frac{\cos E - e}{1-e \cos E} \end{aligned} \right\} \quad (C-13)$$

Thus, given t , (C-11) is used to calculate E , then (C-13) to calculate $\sin v$ and $\cos v$, and (C-12) to calculate θ . The radius vector is given by (C-2).

• Stellar Rotation

The stars are assumed to rotate with orbital period P . The rotational motion is taken to be uniform, even for eccentric orbits, so that the rotation will lag the revolution except on the apse. Thus the rotation angle of the star, θ' , is given by Equation (C-4) with M substituted for v :

$$\theta' = M - \frac{\pi}{2} + \omega \quad (C-14)$$

This produces a small angular deviation between the semi-major axis and the direction to the other star, as shown in Figure 22;

$$\theta = \theta - \theta' = v - M. \quad (C-15)$$

θ' is the angle used in Appendix A.

REFERENCES

1. Chandrasekhar, S., 1933, M.N.R.A.S. 93, 462.
2. Chen, K. Y. and Rhein, W. J., 1969, P.A.S.P. 81, 387.
3. Cochran, V., 1970a, Bull. A. A.S. 2, 304.
4. Cochran, V., 1970b, private communication.
5. Hill, G. and Hutchings, J. B., 1970, Ap. J. 162, 265.
6. Huffer, C. M. and Collins, G. W., II 1963, Ap. J. Suppl. 7, 351.
7. Jurkevich, I., 1964, Machine Reduction, Computation, and Analysis of Light Curves of Eclipsing Binary Systems, General Electric Space Sciences Laboratory R645D8, April 1, 1964.
8. Kopal, J., 1959, Close Binary Systems, (Wiley and Sons, Inc., New York).
9. Kopal, Z., 1968, Ap. and Sp. Sci. 2, 23.
10. Linnell, A. P., 1965, Ap. J. Suppl. 11, 185.
11. Linnell, A. P., 1966, Ap. J. Suppl. 13, 445.
12. Lucy, L. B., 1967, Zs. f. Ap. 65, 89.
13. Lucy, L. B., 1968a, Ap. J. 151, 1123.
14. Lucy, L. B., 1968b, Ap. J. 153, 877.
15. Martin, P. G., 1970, Ap. and Sp. Sci. 7, 119.
16. Merrill, J. E., 1950, Princeton Contr. #23.
17. Russell, H. N., 1912, Ap. J. 35, 315.
18. Russell, H. N., 1948, Harvard Circ. #452.
19. Russell, H. N. and Merrill, J. E., 1952, Princeton Contr. #26.
20. Snowden, M. S. and Koch, R. H., 1969, Ap. J. 156, 667.

21. Tsesevich, V. P., 1939, Bull. Astron. Inst. of U.S.S.R. 45.
22. Tsesevich, V. P., 1940, Bull. Astron. Inst. of U.S.S.R. 50.
23. Walker, R. L. Jr., 1970, A. J. 75, 720.
24. Wood, D. B., 1961, Trans. I.A.U. Vol. XIB, 368.
25. Wood, D. B., 1969, Bull. A.A.S. 1, 267.
26. Wood, D. B., 1971, "A Photometric Study of the Eclipsing Binary Star System RU Ursa Minoris", Bellcomm TM-71-1011-1.
27. Zeipel, H. von, 1924, M.N.R.A.S. 84, 665.

TABLE I

Accuracy of Double Integration
Using the Gauss Method

	Number of Grid Points			
	4 x 4	6 x 6	10 x 10	16 x 16
error with respect to exact value	0.60%	0.19%	0.046%	0.012%
mag. error with respect to 16x16	+0.0036 <u>+0.0009</u>	+0.0002 <u>+0.0003</u>	-0.0002 <u>+0.0001</u>	-----

BELLCOMM, INC.

TABLE II

Comparison with the Spherical Model

Phase	ℓ^{TR}		Phase	ℓ^{OC}	
	Merrill	Wood		Merrill	Wood
.00	.5294	.52941	.50	.6662	.66617
.01	.5464	.54640	.51	.6690	.66902
.02	.6129	.61281	.52	.7060	.70588
.03	.6905	.69067	.53	.7586	.75872
.04	.7672	.76717	.54	.8151	.81511
.05	.8380	.83809	.55	.8698	.86981
.06	.8994	.89952	.56	.9185	.91857
.07	.9487	.94871	.57	.9582	.95829
.08	.9832	.98325	.58	.9864	.98640
.09	.9995	.99982	.59	.9996	.99986

TABLE III

Parameters For Systems Discussed In Text

Elements	"standard"	VZ Hydrae	EG Cepheii	V1143 Cygni	RU Ursa Minoris	Phase Shift
i	88.0°	89.25°	84.75°	87.02°	83.0°	73.1°
a	0.20	0.119	0.472	0.055	0.480	0.47
k	1.50	0.84	0.663	1.11	0.564	0.80
j	0.75	0.835	0.125	0.952	0.020	0.20
ϵ_A	0.994	1.0	0.914	1.0	0.953	0.95
ϵ_B	0.924	1.0	0.914	1.0	0.932	0.95
ζ_A	0.012	0	0.040	0	-0.017	0
ζ_B	0.038	0	0.060	0	0.038	0
u_A	0.6	0.6	0.6	0.68	0.89	0.6
u_B	0.6	0.6	0.8	0.68	1.0	0.6
v_A	-4.0	0	-2.9	0	-4.6	-4.0
v_B	-4.0	0	-5.2	0	-7.5	-4.0
w_A	0	0	0	0	0.33	1.0
w_B	0	0	0	0	0.33	1.0
e sin ω	0	0	0	.4046	0	0
e cos ω	0	0	0	.3609	0	0

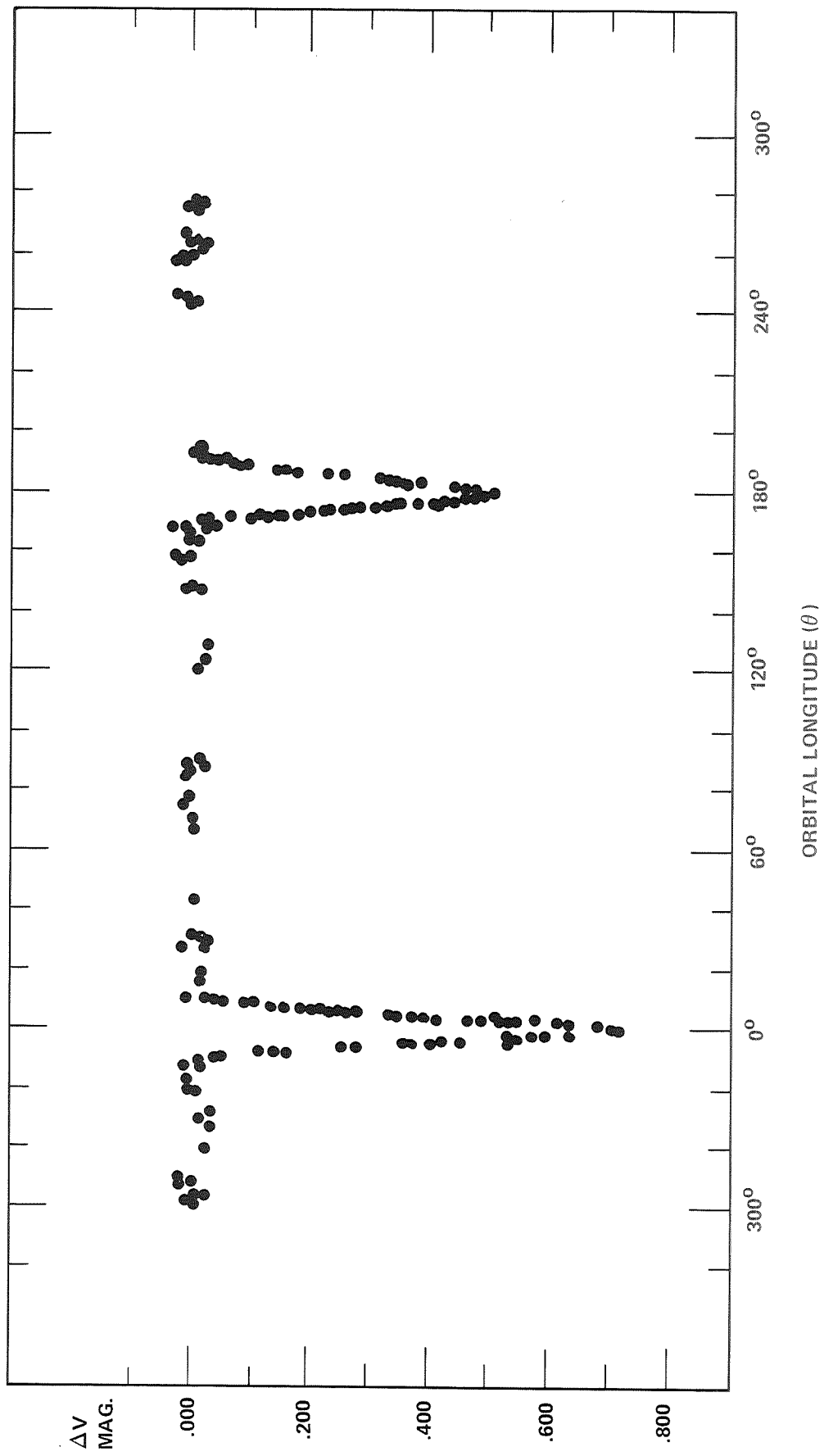


FIGURE 1. A TYPICAL LIGHT CURVE; THE ECLIPSING STAR VZ HYDRAE (OBSERVED BY D. WALKER).

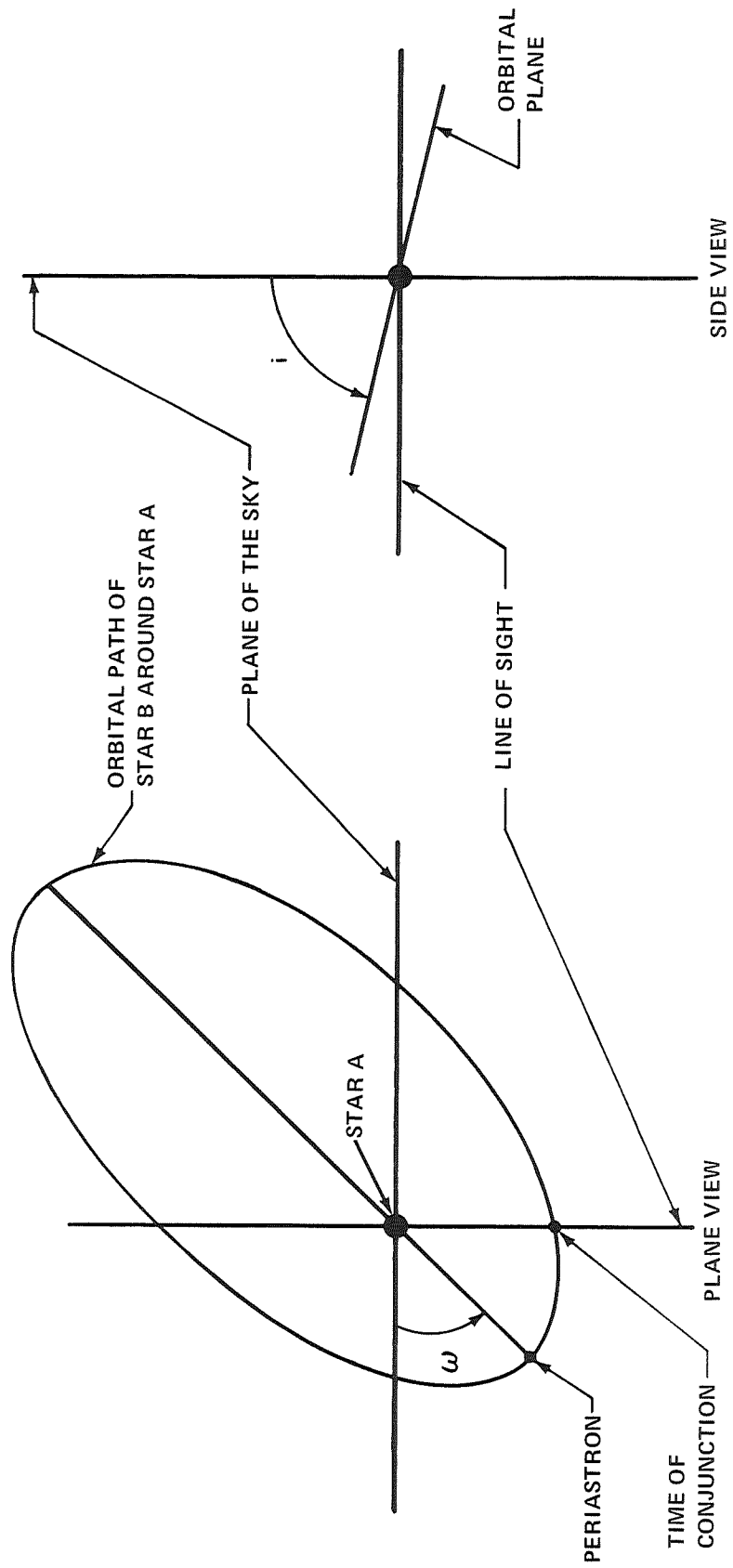


FIGURE 2 - ORBITAL PARAMETERS

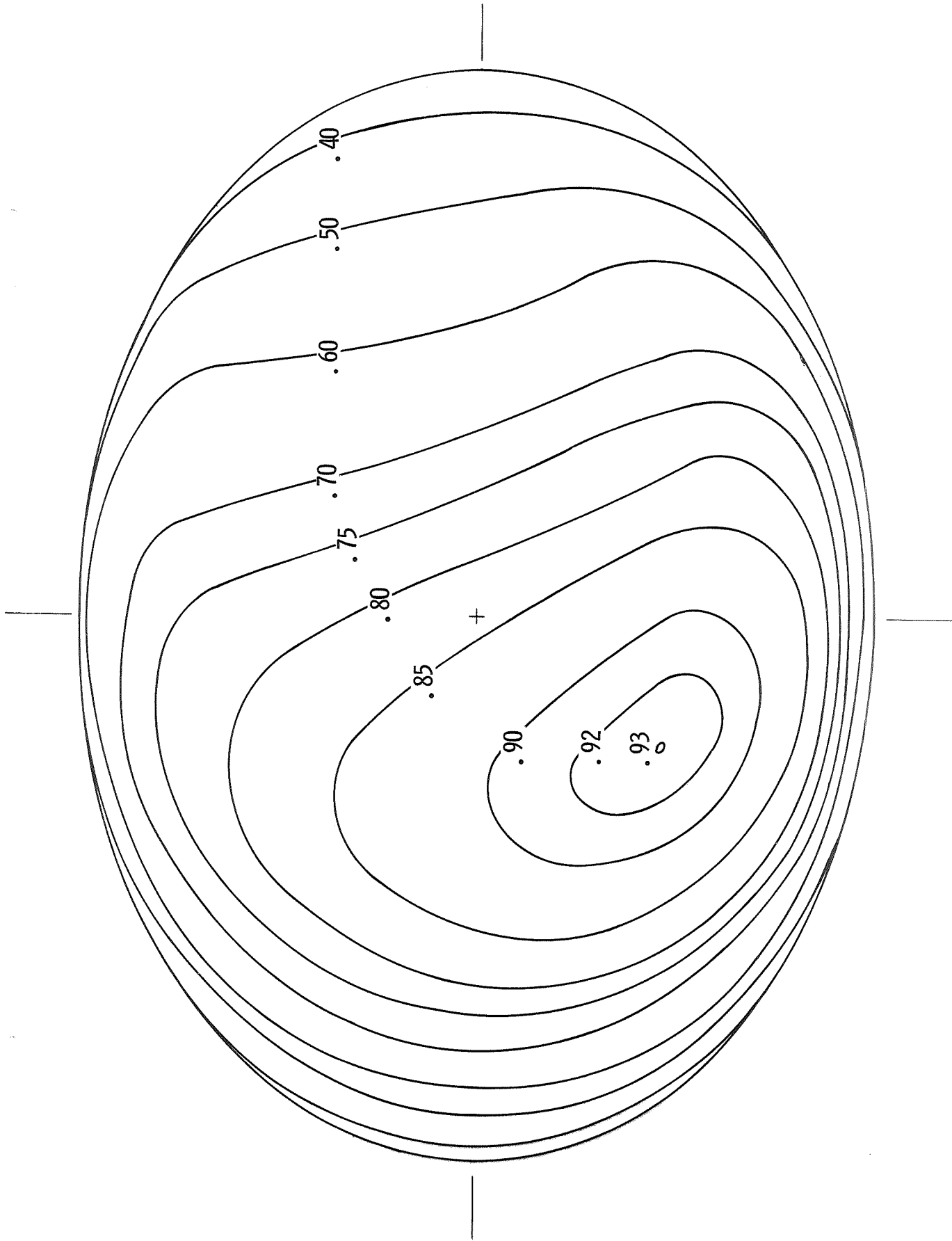


FIGURE 3 - TYPICAL ISOPHOTAL COUNTOURS ON A DISTORTED STAR.
COUNTORS ARE LABELED WITH RESPECT TO THE SUB-EARTH POINT
AT QUADRATURE.

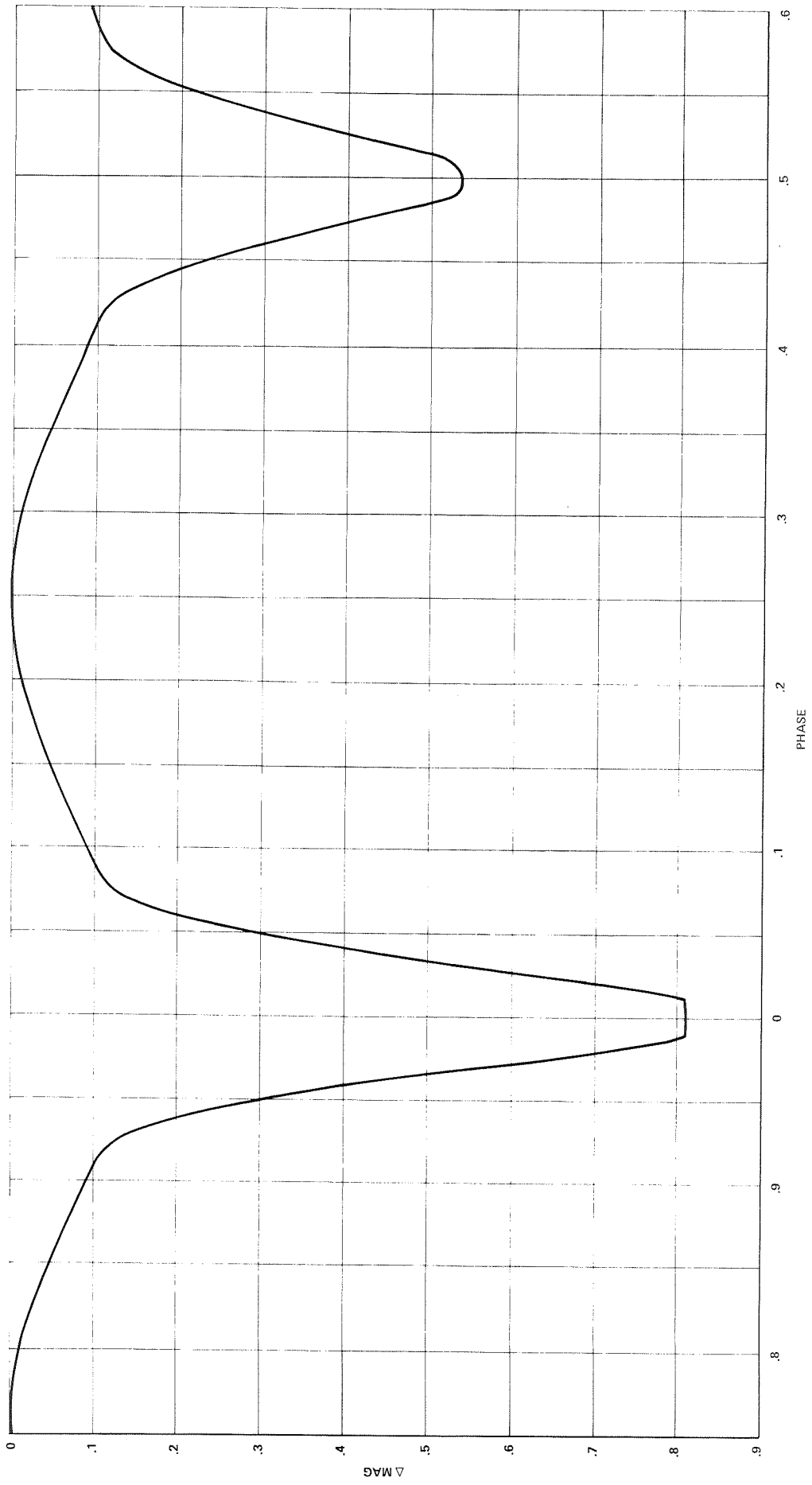


FIGURE 4. REFERENCE THEORETICAL LIGHT CURVE. OTHER THEORETICAL CURVES IN THIS SECTION WILL BE BASED ON THIS ONE.

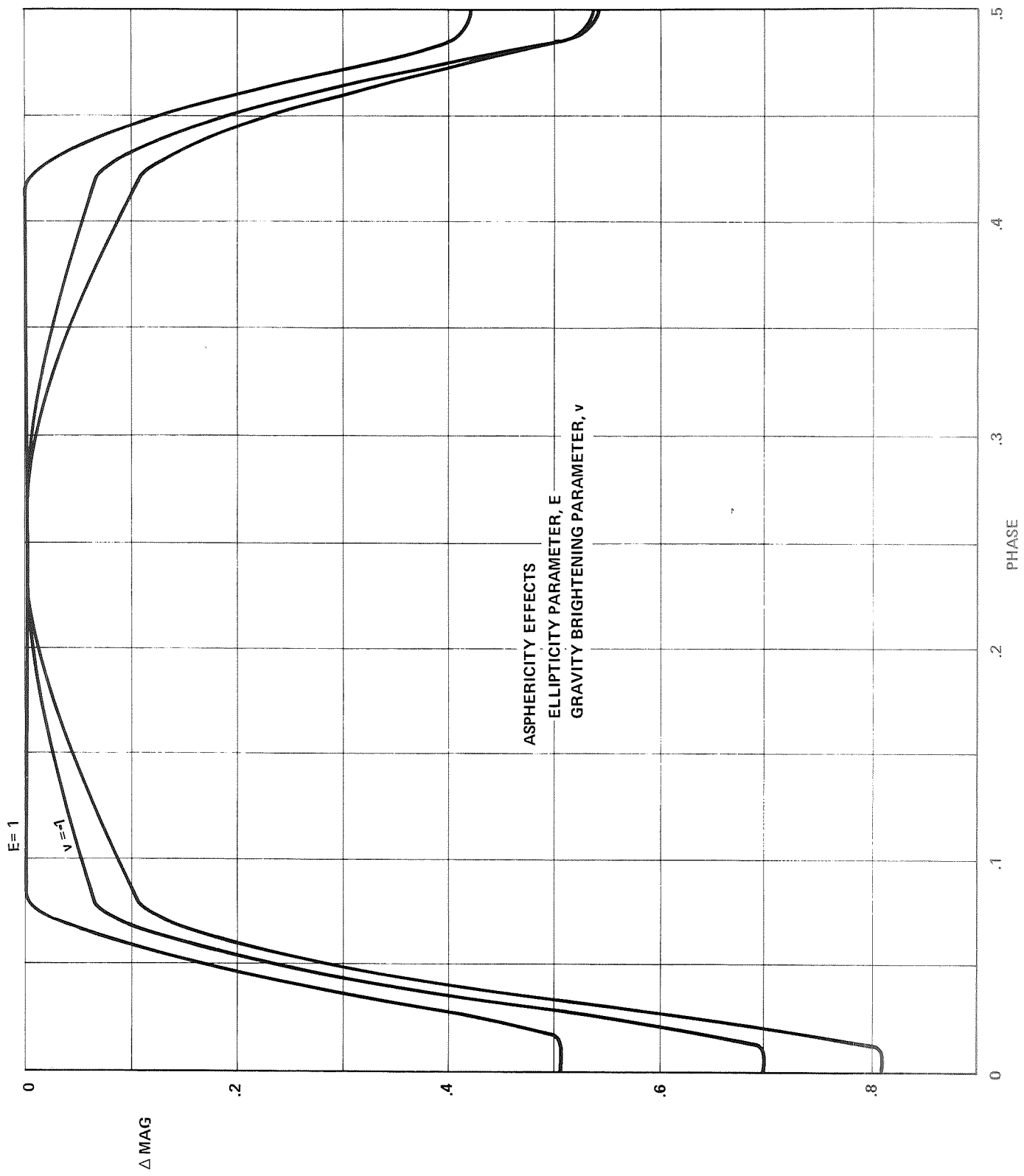


FIGURE 5. EFFECT OF ASPHERICITY. TOP CURVE IS FOR SPHERICAL STARS;
 NEXT CURVE IS FOR GRAVITY BRIGHTENING PARAMETER
 $v = -1$; BOTTOM CURVE IS REFERENCE.

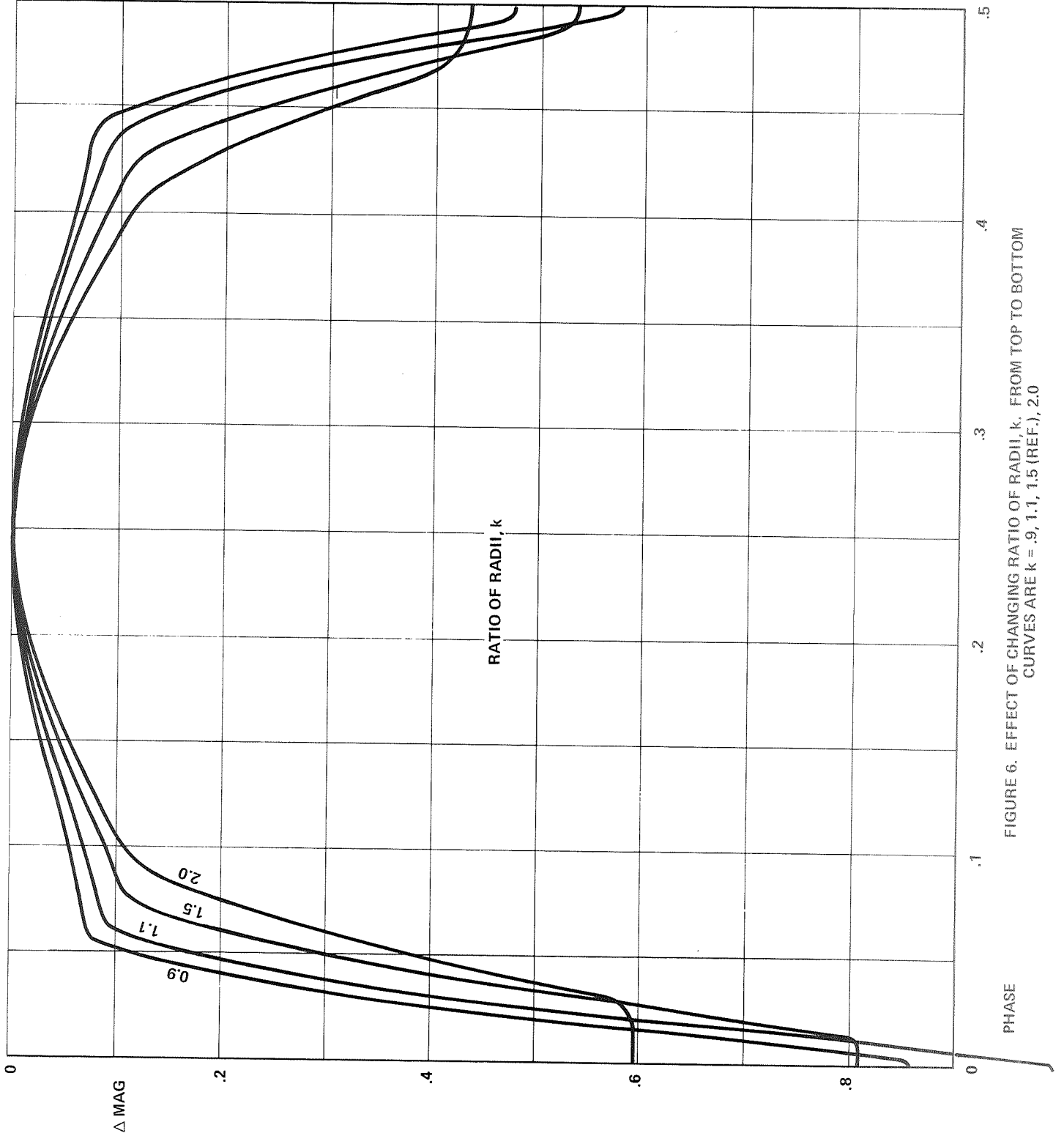


FIGURE 6. EFFECT OF CHANGING RATIO OF RADII, k . FROM TOP TO BOTTOM CURVES ARE $k = .9, 1.1, 1.5$ (REF.), 2.0

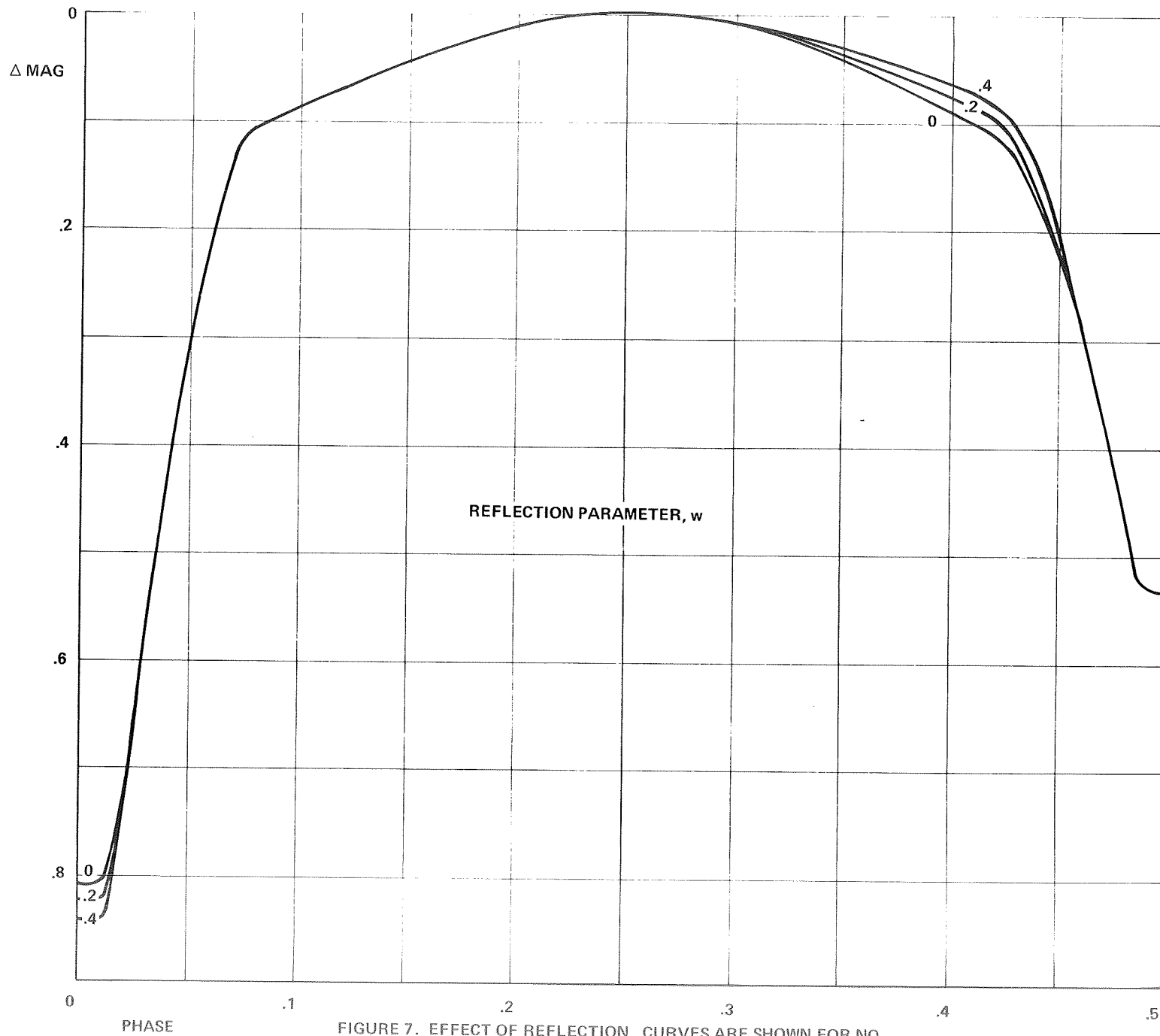


FIGURE 7. EFFECT OF REFLECTION. CURVES ARE SHOWN FOR NO REFLECTION (REF.), AND $w = .2$ AND $.4$.

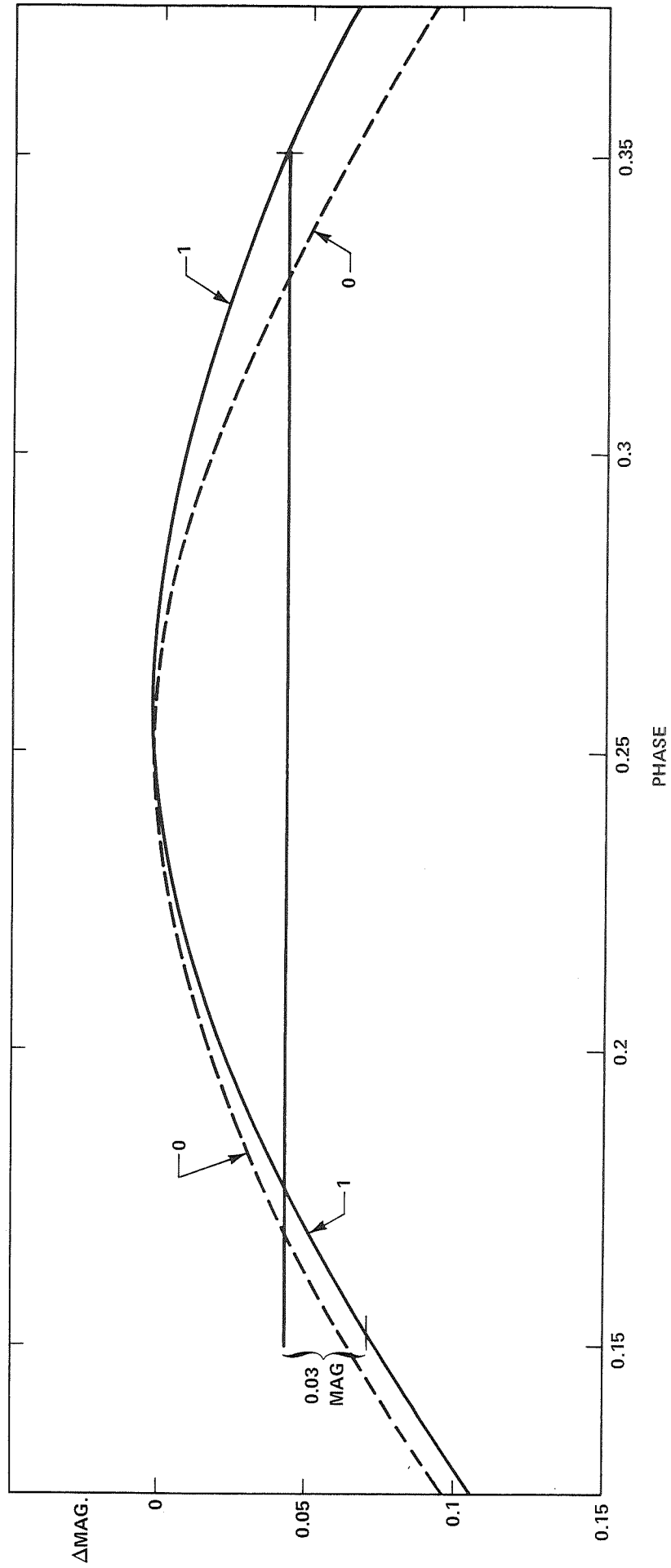


FIGURE 8 - REFLECTION EFFECTS ON SHOULDERS OF CLOSE STARS. THIS IS FOR STARS WHICH ARE CLOSER TOGETHER THAN THOSE IN THE REFERENCE SYSTEM

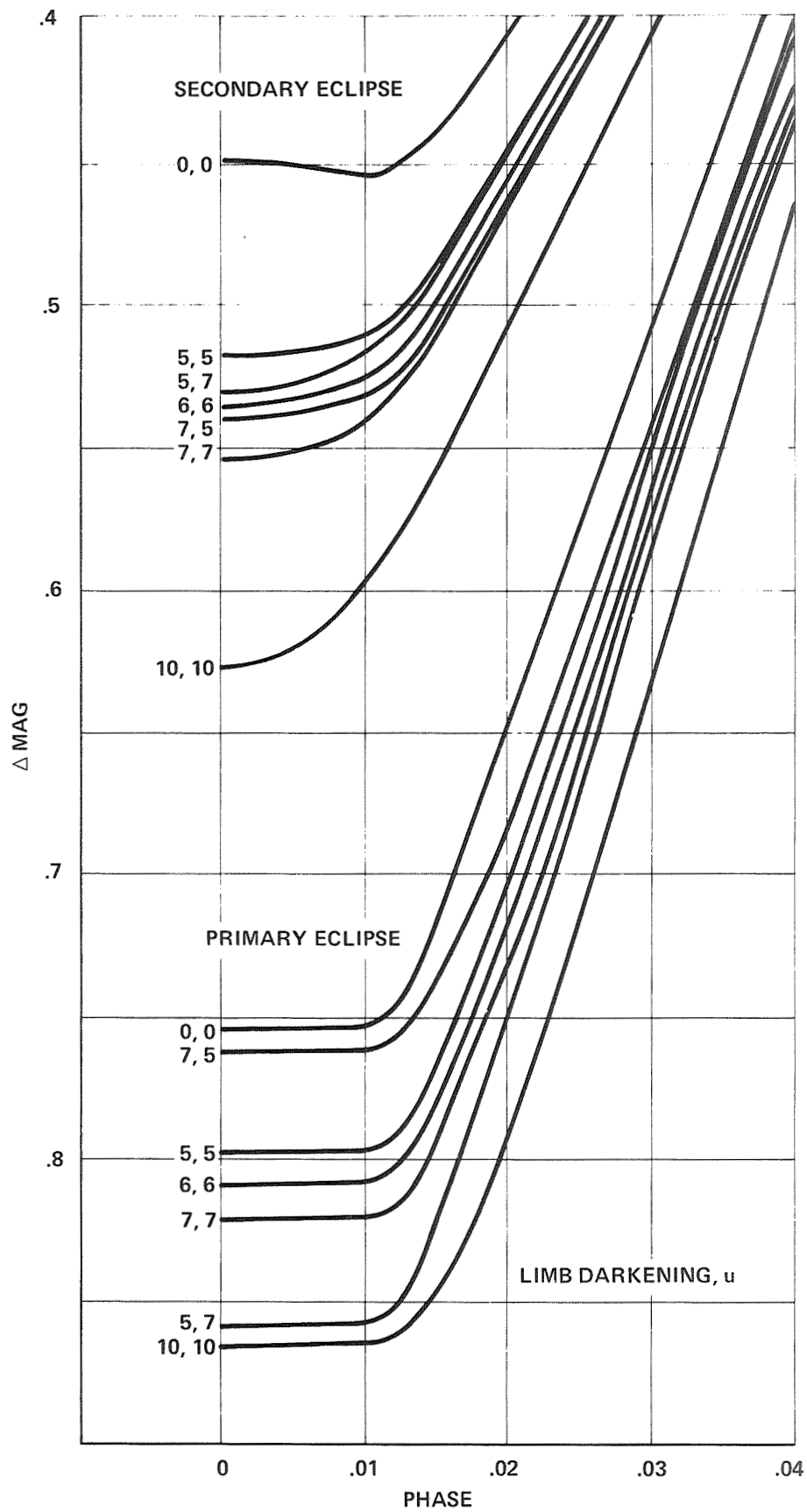


FIGURE 9. EFFECT OF LIMB DARKENING. CURVES ARE LABELED WITH $10 \times u_A$ and $10 \times u_B$.

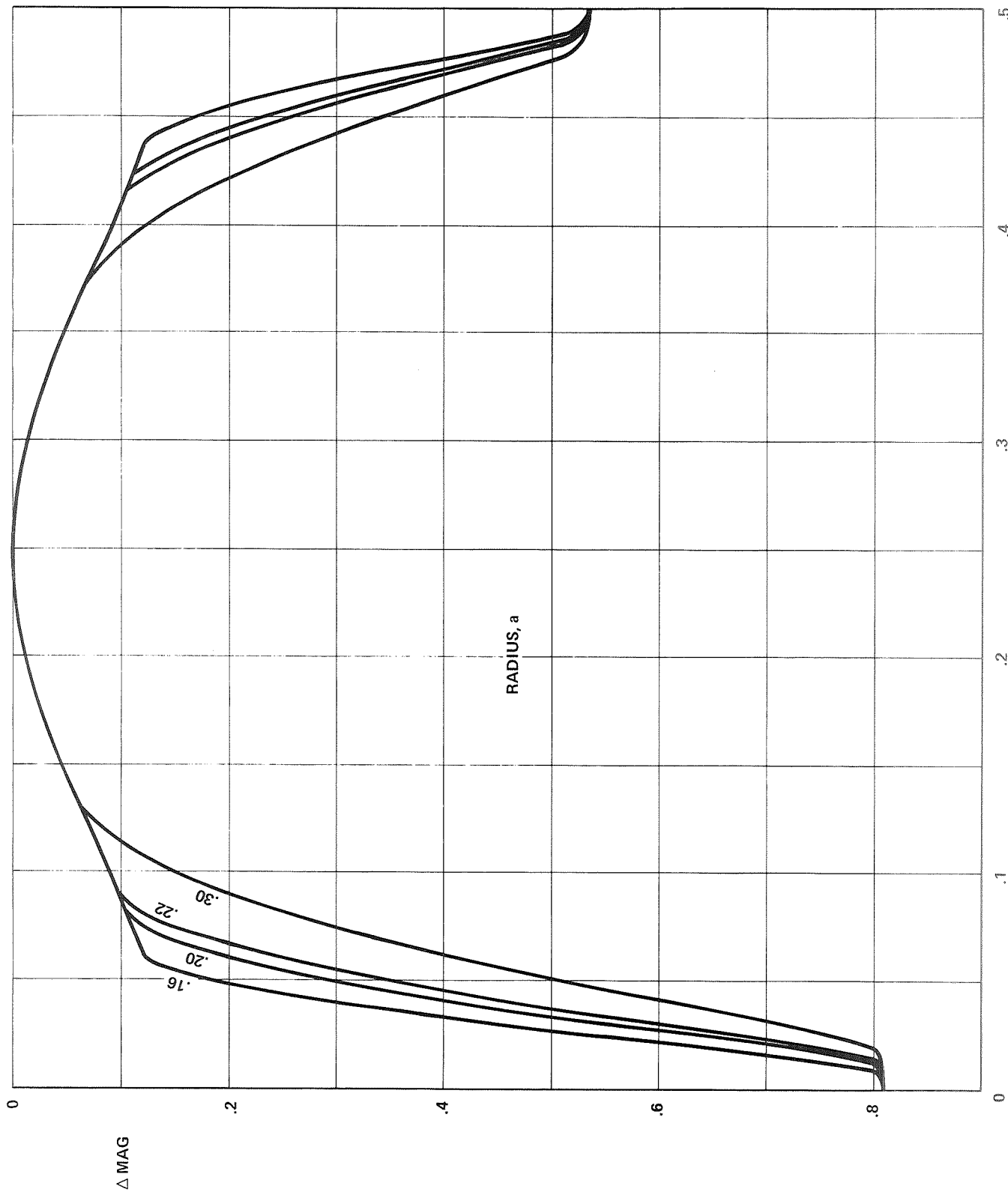


FIGURE 10. EFFECT OF CHANGING RADIUS PARAMETER, a . FROM TOP TO BOTTOM, CURVES ARE $a = .16, .20$ (REF.), $.22, .30$.

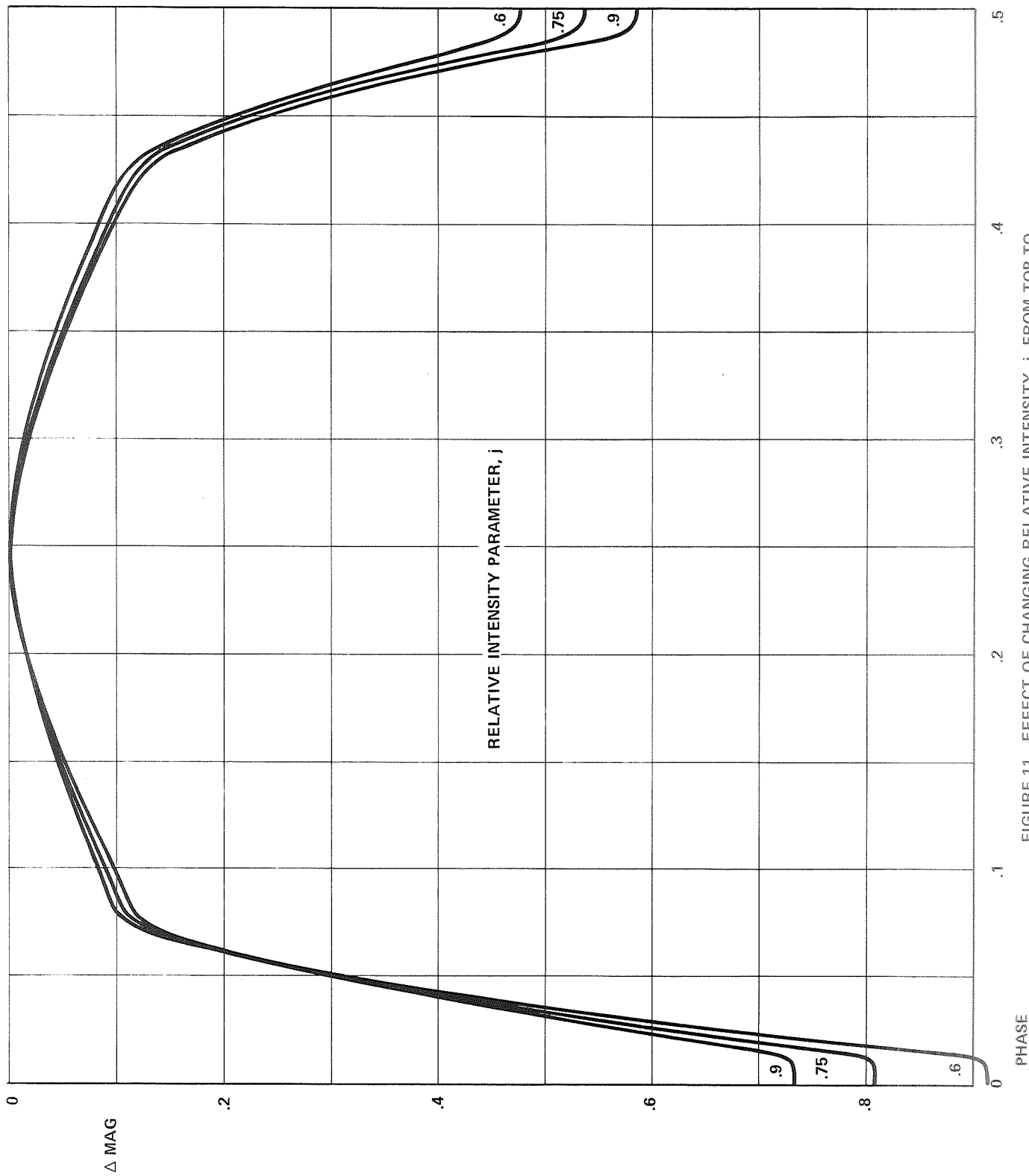


FIGURE 11. EFFECT OF CHANGING RELATIVE INTENSITY, j , FROM TOP TO BOTTOM (IN PRIMARY ECLIPSE) CURVES ARE $j = .9, .75$ (REF), $.6$.

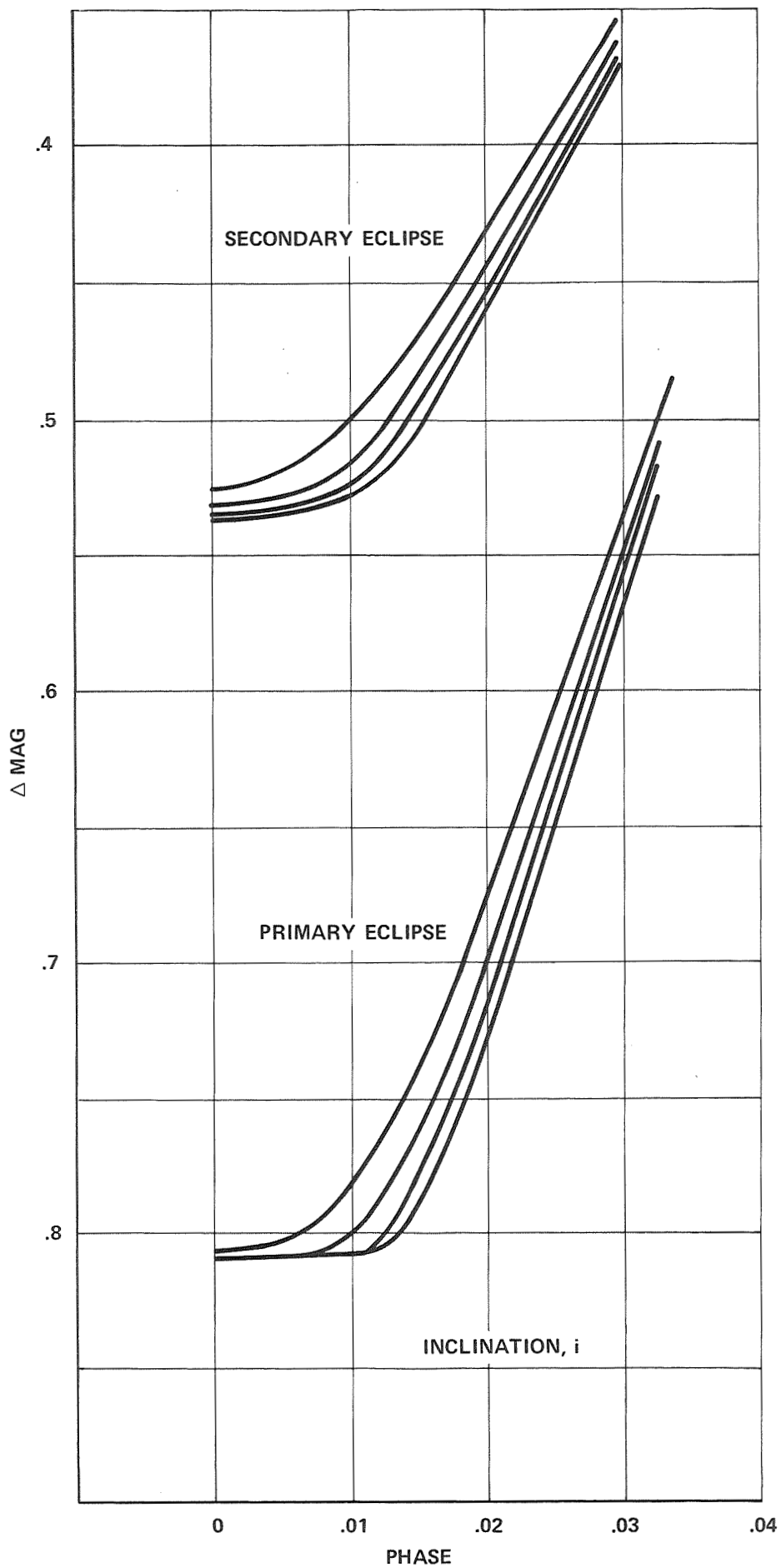


FIGURE 12. EFFECT OF INCLINATION NEAR 90° . FROM TOP TO BOTTOM IN EACH ECLIPSE, CURVES ARE $i = 86^\circ, 87^\circ, 88^\circ$ (REF.), 90° .

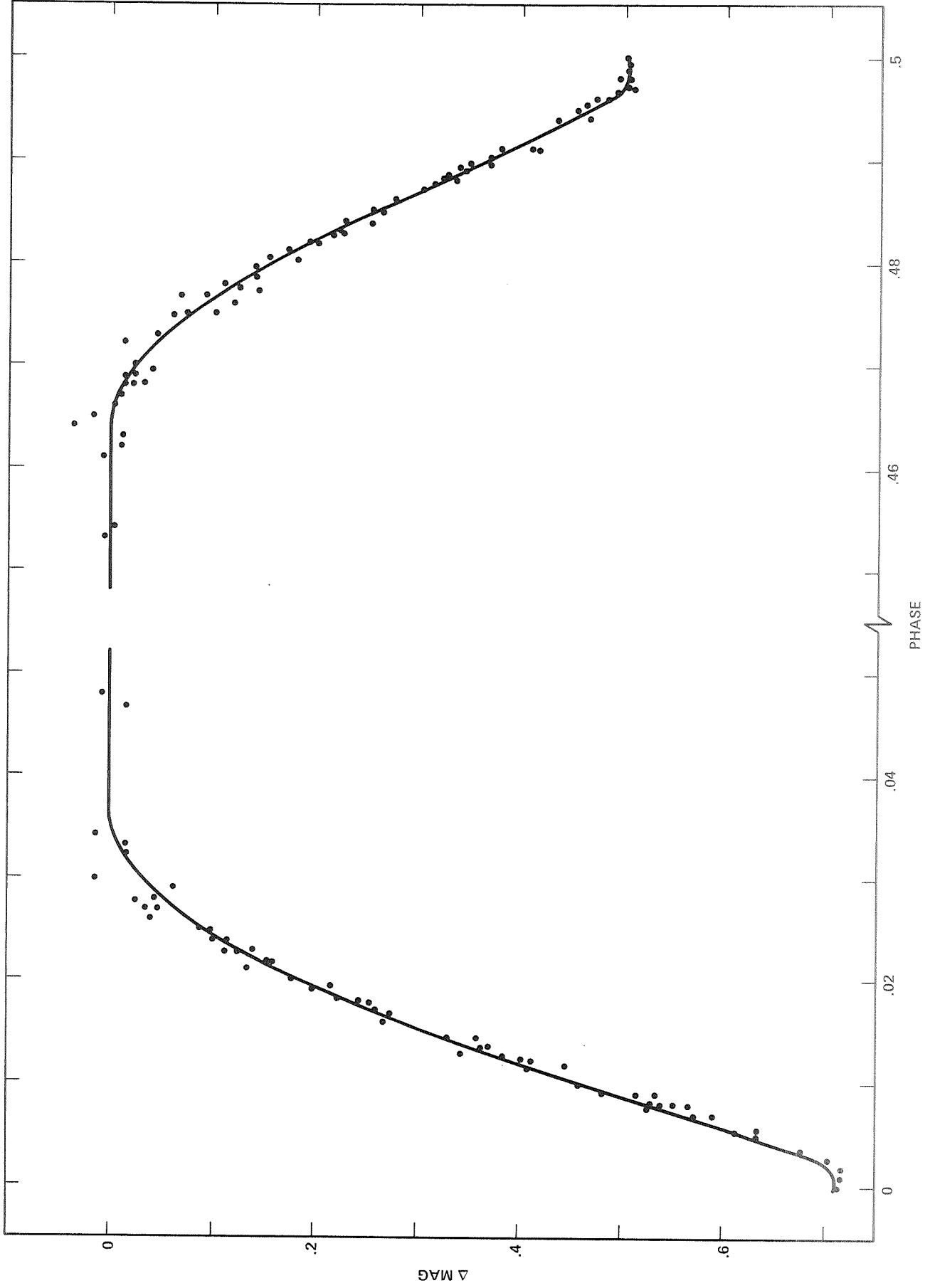


FIGURE 13 - FIT TO OBSERVATIONS OF VZ HYDRAE. THE ECLIPSES HAVE BEEN FOLDED ABOUT THEIR CENTERS, SUPERIMPOSING DESCENDING AND ASCENDING BRANCHES

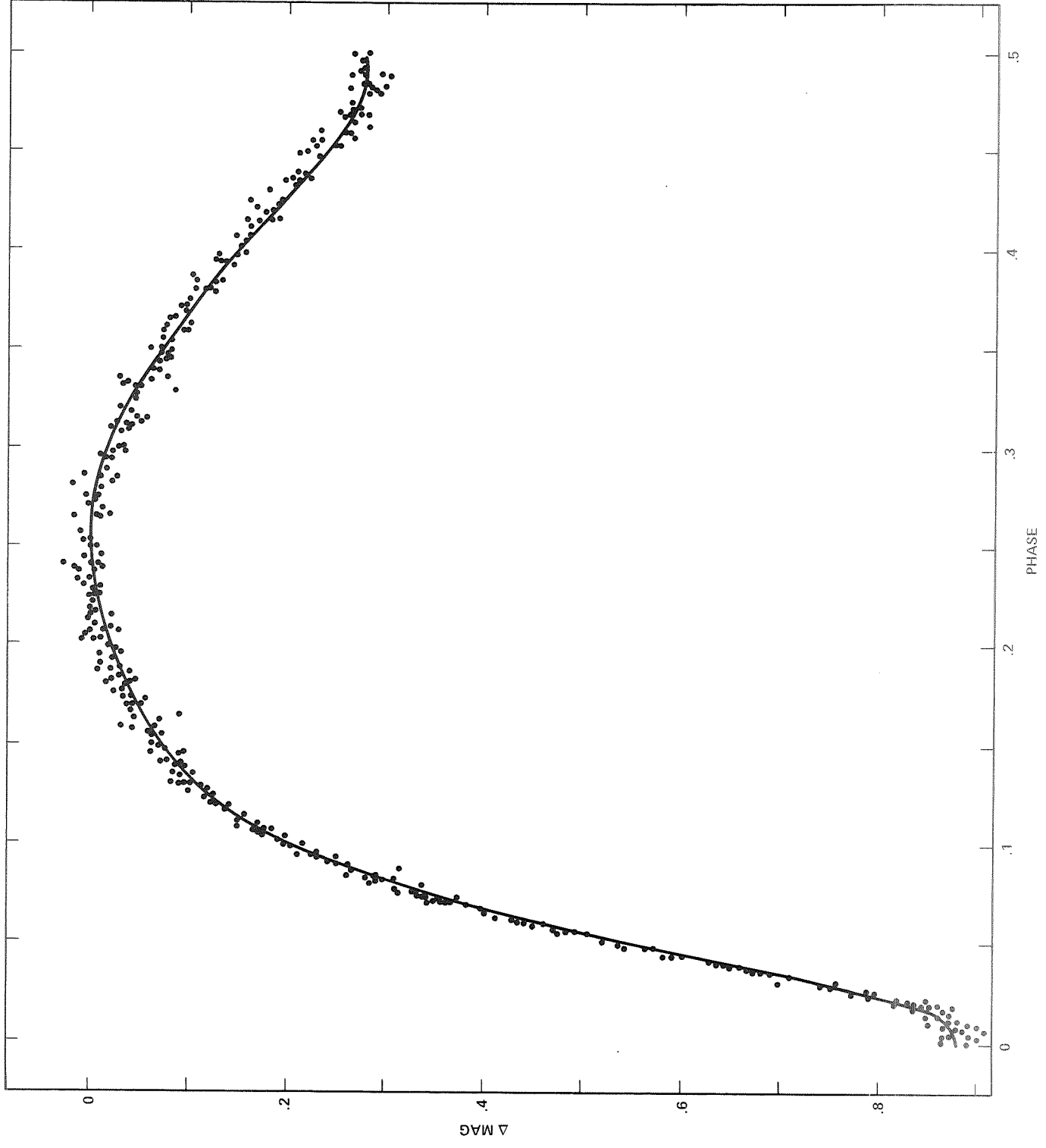


FIGURE 14 - FIT TO OBSERVATIONS OF EG CEPHEI

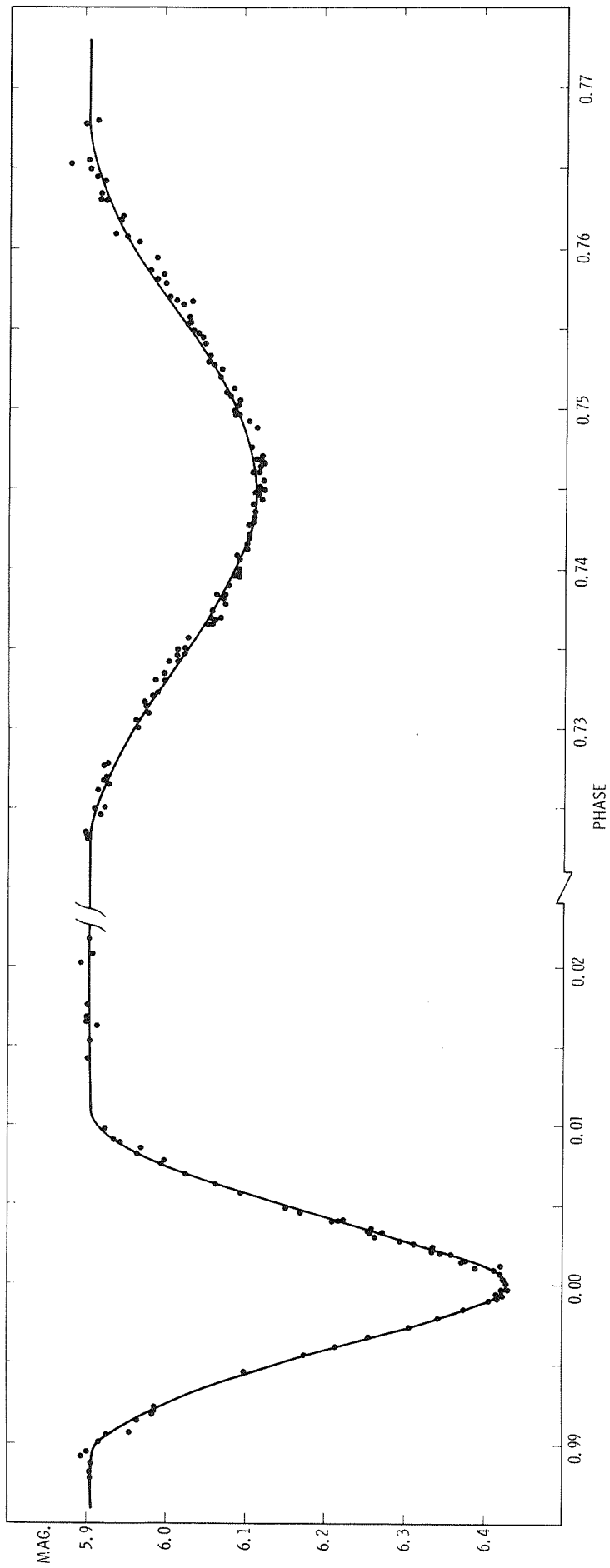


FIGURE 15 - FIT TO OBSERVATIONS OF V1143 CYGNI.

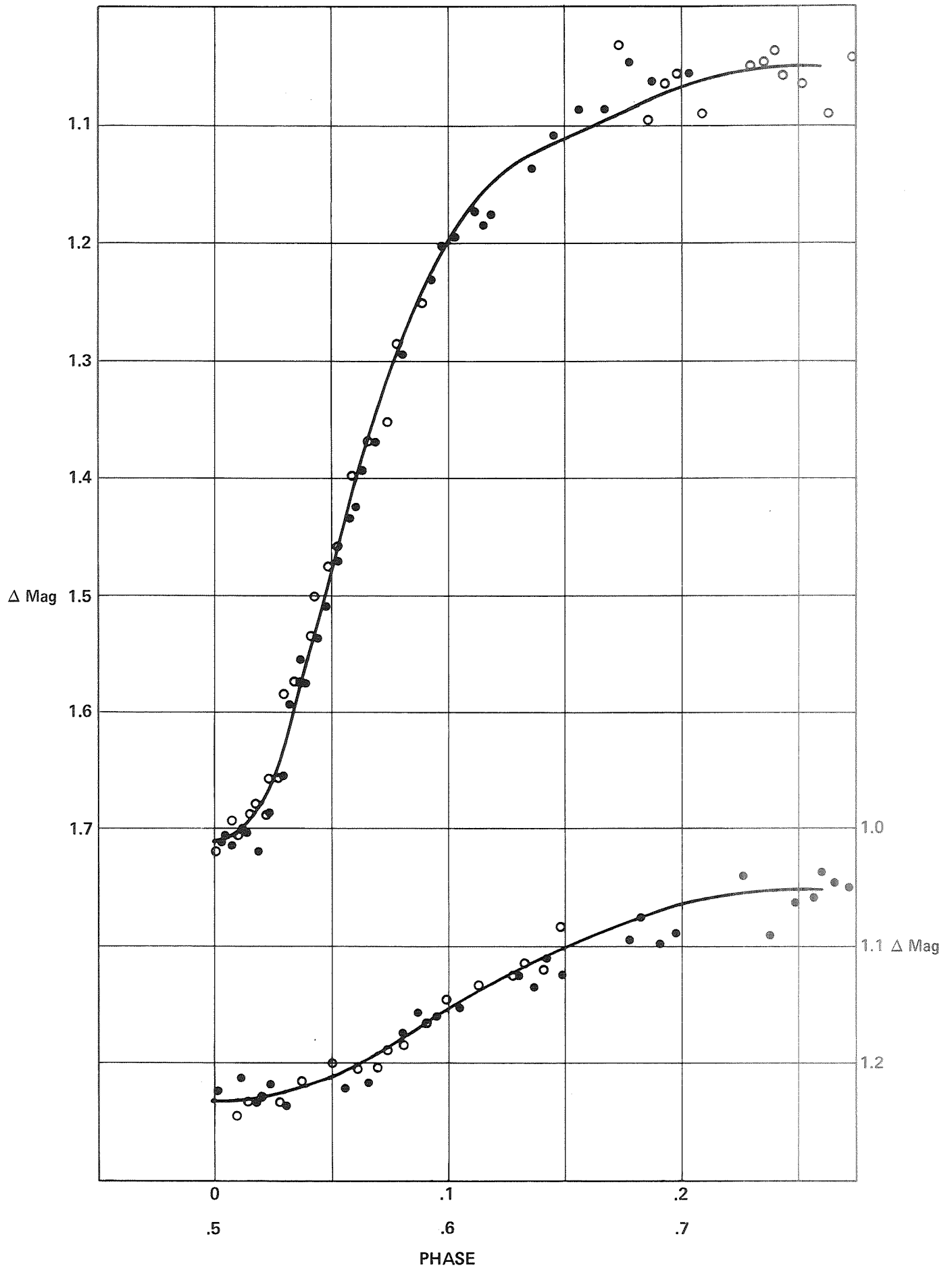


FIGURE 16 - FIT TO OBSERVATIONS OF RU UMi

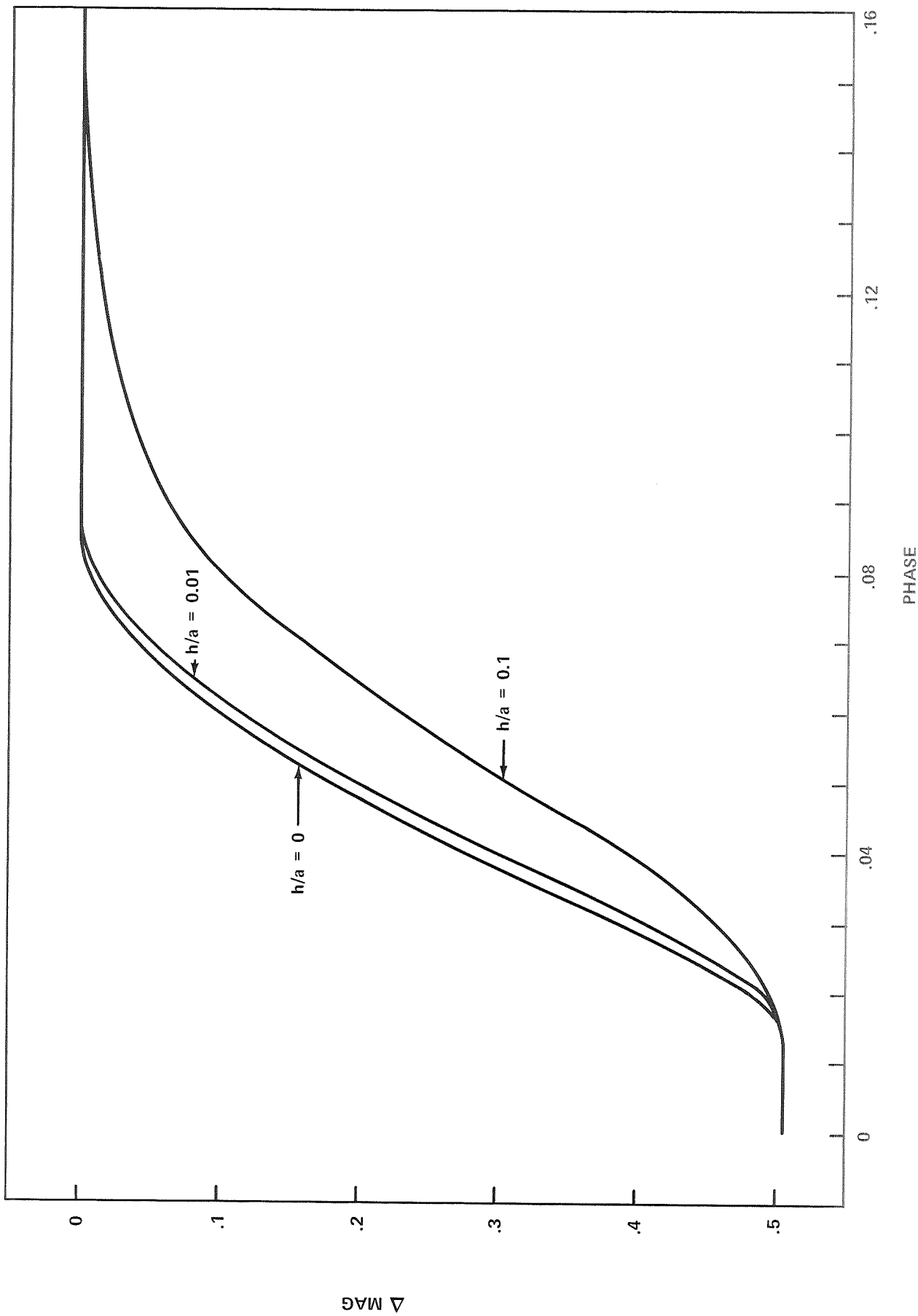


FIGURE 17 - THE EFFECT OF AN ABSORBING ATMOSPHERE AROUND THE ECLIPSING STAR IS TO BROADEN THE ECLIPSE.

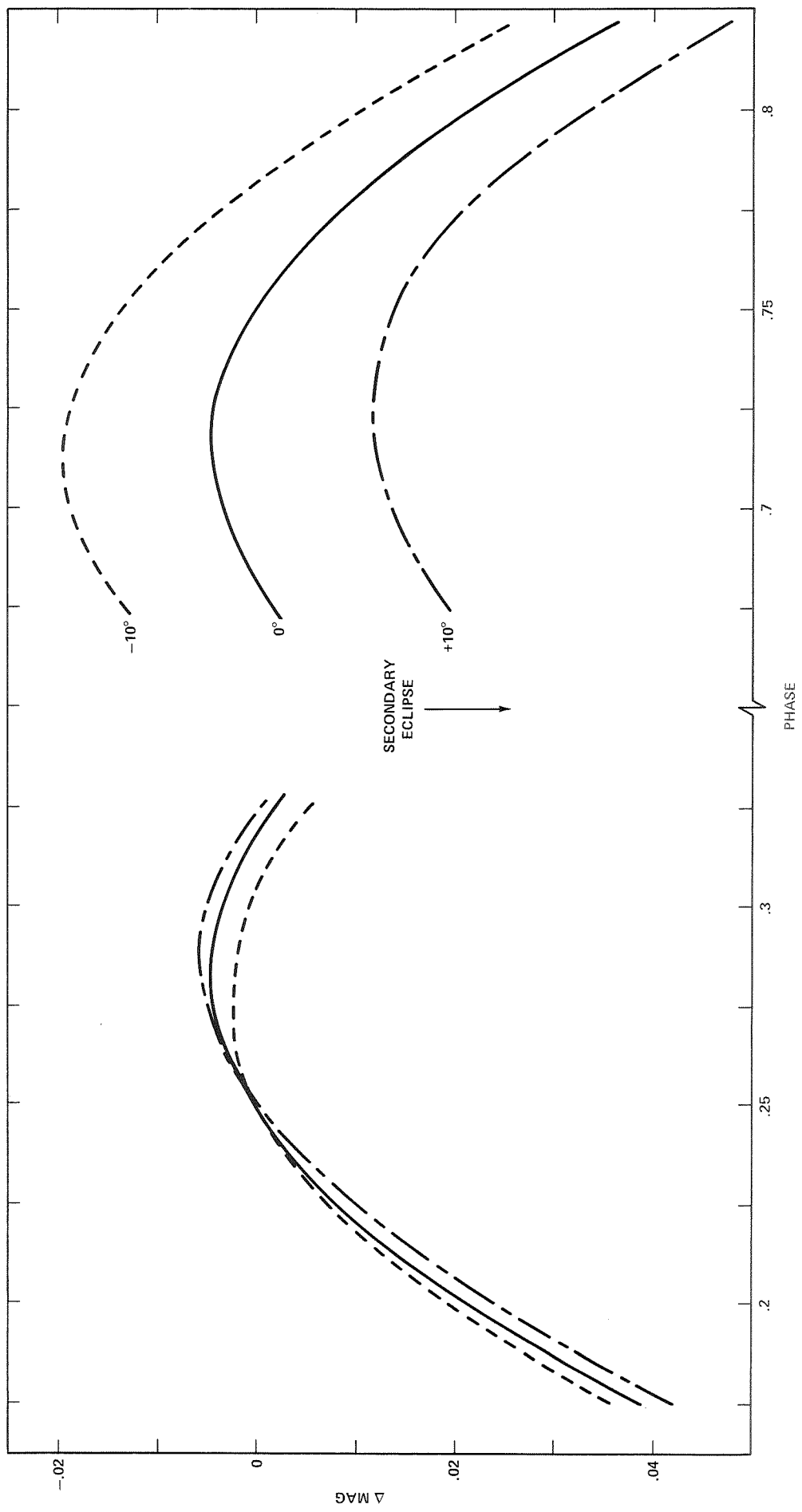


FIGURE 18 - ASYMMETRY INTRODUCED BY LEAD OR LAG IN PHASE OF REFLECTION. ONLY QUADRATURES ARE SHOWN IN THIS DETAIL. NORMALIZATION HAS FORCED ALL CURVES THROUGH 0 AT PHASE 0.25

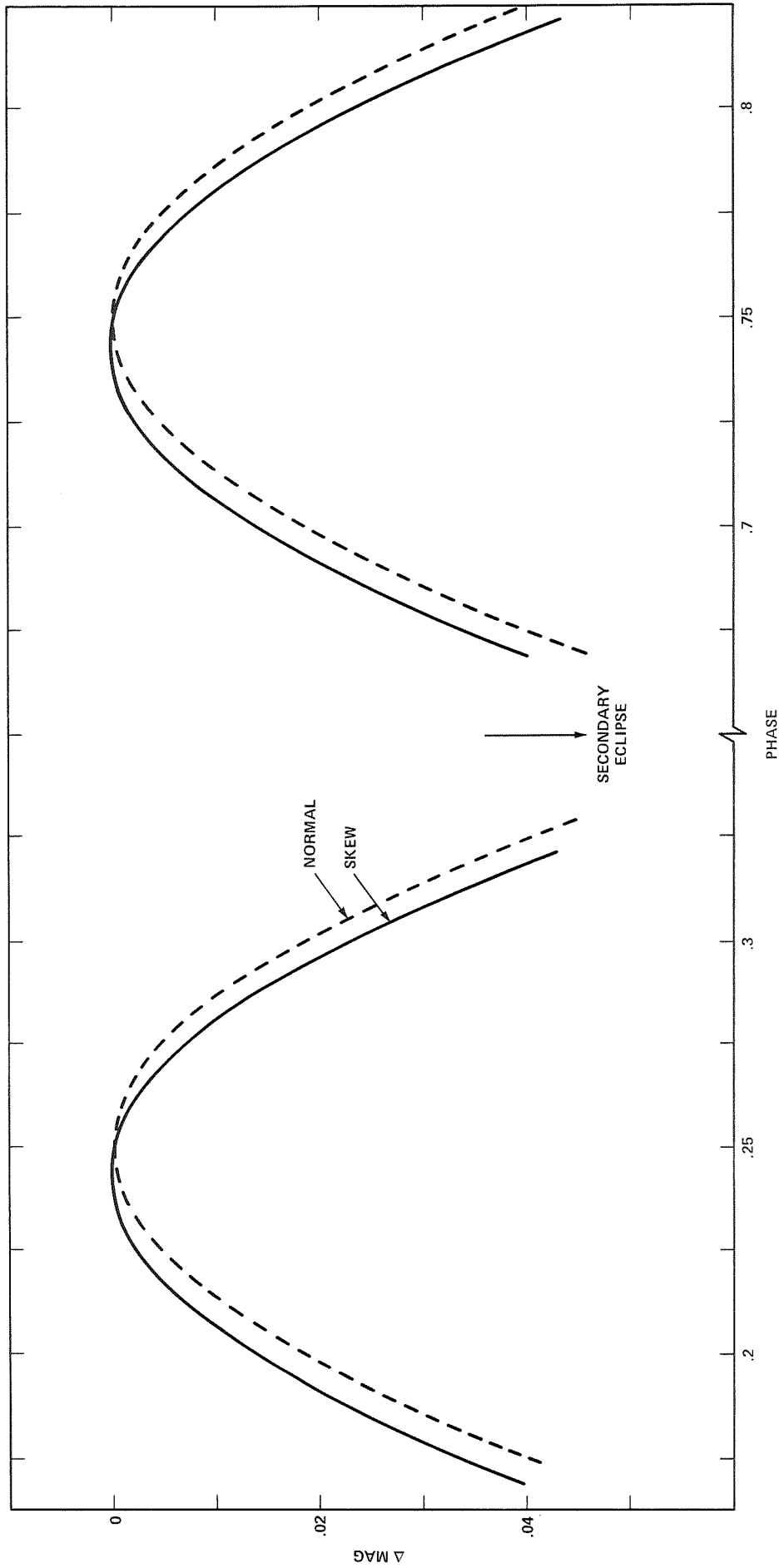


FIGURE 19 - EFFECT OF STARS SKEW TO ORBITAL PLANE. PRIMARY STAR IS INCLINED 5° FROM PLANE AND ITS ROTATION LEADS REVOLUTION BY 5°

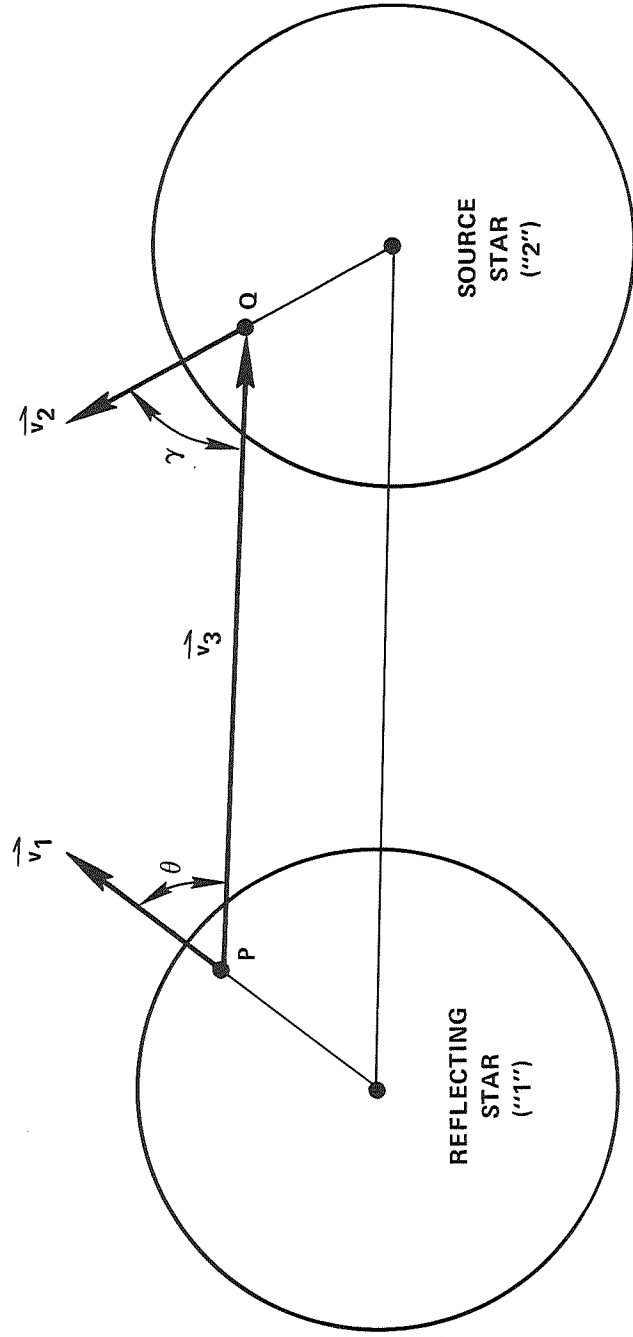


FIGURE 20. THE GEOMETRY OF THE REFLECTION EFFECT IS IMBODIED IN THE 3 VECTORS v_1, v_2, v_3 .

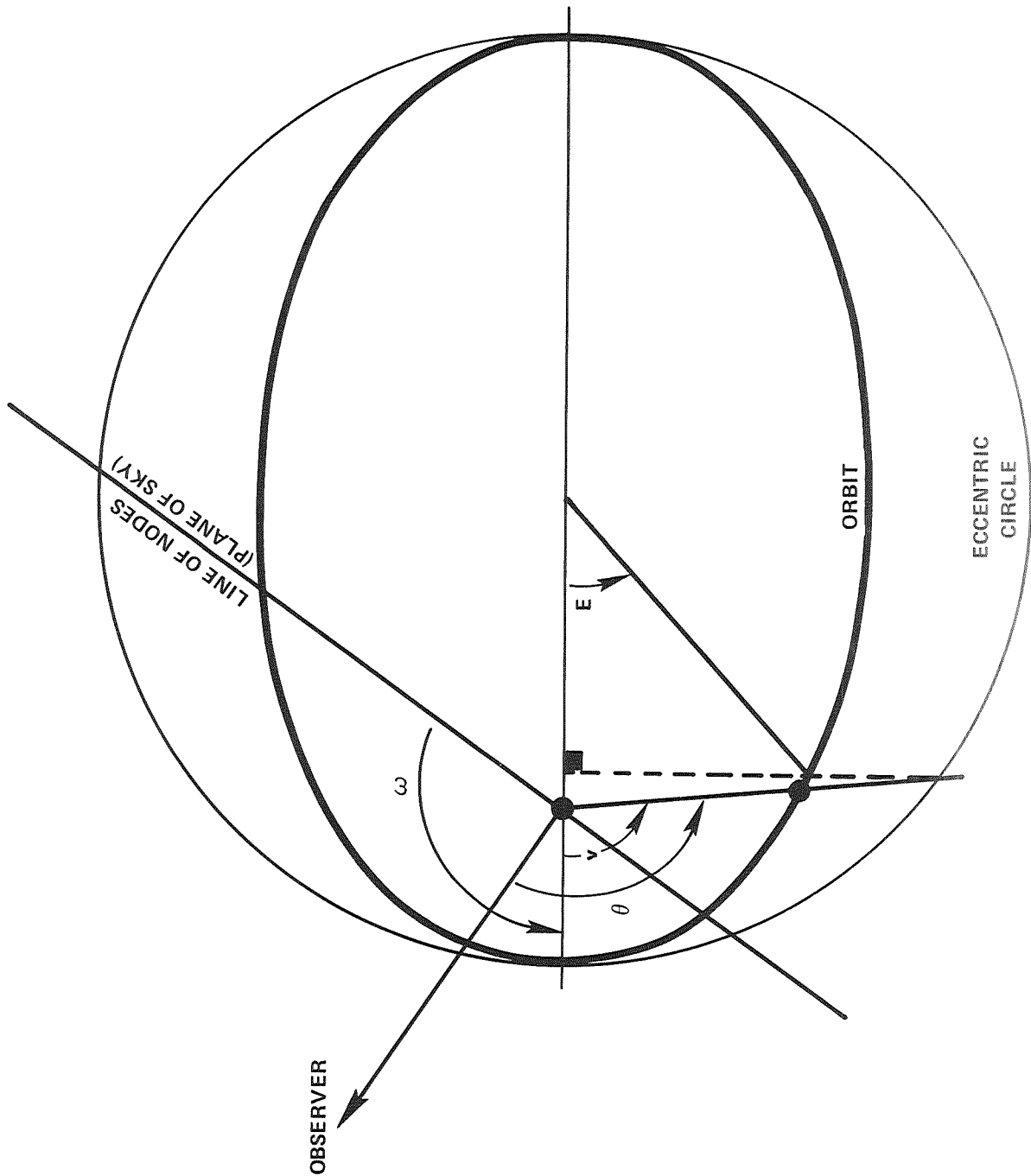


FIGURE 21. PLANE VIEW OF ORBIT, SHOWING RELATIONSHIPS BETWEEN θ , ω , ν , AND E .

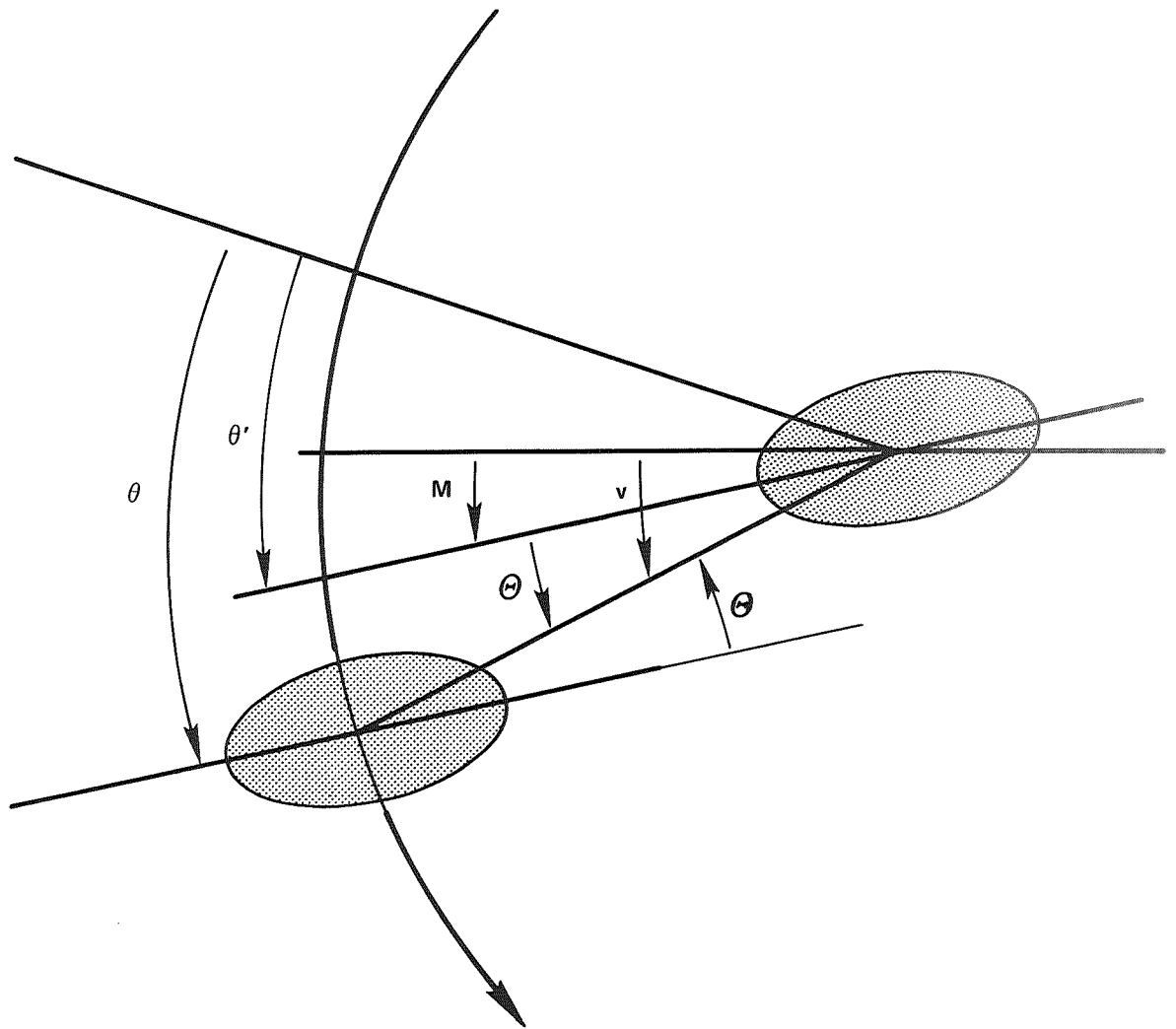


FIGURE 22. IN AN ECCENTRIC ORBIT, ROTATION AND REVOLUTION MAY NOT COINCIDE;

θ MEASURES THE DISPARITY.